






Sensitivity of Real-Time Forecast for Typhoons Around Korea to Cumulus and Cloud Microphysics Schemes

Jinyoung Park¹, Jihong Moon¹, Woojin Cho¹, Dong-Hyun Cha¹ , Myong-In Lee¹ , Eun-Chul Chang² , Joowan Kim² , Sang-Hun Park³ , and Jooneun An⁴

¹Department of Urban & Environmental Engineering, Ulsan National Institute of Science and Technology, Ulsan, Korea, ²Department of Atmospheric Sciences, Kongju National University, Gongju, Korea, ³Department of Atmospheric Sciences, Yonsei University, Seoul, Korea, ⁴Korea Institute of Science and Technology Information, Daejeon, Korea

Key Points:

- The effect of cumulus parameterization and cloud microphysics schemes on the real-time forecast of typhoons around South Korea is studied
- One of the cumulus parameterization schemes was modified to decrease its activity at low latitudes
- Even short-term typhoon forecasts could be largely affected by the forecast performances of convective processes at the tropics

Supporting Information:

Supporting Information may be found in the online version of this article.

Correspondence to:

D.-H. Cha,
dhcha@unist.ac.kr

Citation:

Park, J., Moon, J., Cho, W., Cha, D.-H., Lee, M.-I., Chang, E.-C., et al. (2023). Sensitivity of real-time forecast for typhoons around Korea to cumulus and cloud microphysics schemes. *Journal of Geophysical Research: Atmospheres*, 128, e2022JD036709. <https://doi.org/10.1029/2022JD036709>

Received 28 FEB 2022
Accepted 13 JAN 2023

Abstract In numerical weather prediction models, the typhoon track and intensity forecast performances are highly sensitive to physics parameterization schemes. To investigate the impact of physics parameterization schemes on the real-time short-term forecasts, we simulated six typhoons which directly/indirectly affected the South Korea region in recent years using the Weather Research and Forecasting (WRF) model. Three cumulus parameterization schemes (CPSs) of Kain-Fritsch (KF), Betts-Miller-Janjić (BMJ), modified Tiedtke (TDK), and two cloud microphysics parameterization schemes (MPSs) of WRF-single-moment-microphysics class 6 (WSM6), Predicted Particle Properties (P3) 1-category were selected for the sensitivity experiment. The results showed that there was a significant difference in simulated typhoon track and intensity performances depending on the physics schemes. On average, the typhoon forecast performances were improved when applying the KF scheme for CPS and WSM6 scheme for MPS in our experimental setup. The BMJ-applied runs showed the worst performances, which simulated westward shifted typhoon tracks compared to other runs. Overall, the typhoon track and intensity spreads tended to be more sensitive to CPSs and MPSs, respectively. We conducted additional sensitivity experiments using the BMJ scheme with modified reference and temperature profiles. The result showed that the overactivity of the BMJ scheme at low latitudes was reasonably reduced, leading to the improved simulation of typhoons and synoptic fields.

Plain Language Summary To improve the real-time short-term forecast performances for the recent typhoon cases that affected South Korea, sensitivity experiments for the various physics parameterization schemes, such as cumulus parameterization and cloud microphysics schemes, were conducted. Through additional experiments with one of the modified schemes and a comparison of detailed inner cloud processes, the reason for the different track and intensity forecast performances among the sensitivity experiments were revealed.

1. Introduction

Recently, the frequency of tropical cyclones (TCs) affecting East Asia has been increasing (Chang et al., 2021; J.-W. Choi, Cha, & Kim, 2017; Choi & Kim, 2007; Choi & Moon, 2012; Kim, 2008; Lee et al., 2019; Lee et al., 2012; Liu et al., 2020; Park et al., 2014; Tu et al., 2009; Wu et al., 2005); moreover, intense TCs have become stronger owing to the global warming (Cha et al., 2014; Elsner et al., 2008; Holland & Bruyère, 2014; Knutson et al., 2010; Murakami et al., 2012, 2015; Webster et al., 2005; Wu & Zhao, 2012). In particular, a number of TCs maintain their intensity before making landfall, allowing them to cause widespread damage and trigger enormous economic loss. This is a serious problem for coastal populations. Mitigating TC hazards and risk in advance, it is necessary to improve the short-term forecast performance of TCs. Since operational global models have been upgraded in many fields (i.e., developing data assimilation/ensemble technique, increasing horizontal resolution, and upgrading physics packages), their forecast performances have steadily improved. However, even short-term (3 days or less) TC predictions still have track errors of hundreds of kilometers (Cangialosi, 2020; Goerss, 2007; Landsea & Cangialosi, 2018; Munsell et al., 2015; Sakai & Yamaguchi, 2005; Tang et al., 2021; Xu et al., 2016; Yamaguchi et al., 2017; Zhou et al., 2017) and/or inability to simulate rapid intensification (weakening) of TCs (Cangialosi, 2020; DeMaria et al., 2021; Elsberry et al., 2007; Gopalakishnan et al., 2021; Na et al., 2018; Trabling & Bell, 2020; Wood & Ritchie, 2015). The uncertainties in short-term typhoon track prediction also occur in high-resolution regional operational models (Chen et al., 2019; Heming et al., 2019).

Yamaguchi et al. (2017) showed that those large TC track errors of short-term forecasts tend to be affected by some TC cases, which have extremely large forecast errors.

It is known that TC track is largely affected by the surrounding synoptic fields. However, they can also be affected by TC-related circulation (i.e., the beta effect) as they have different sizes and intensities (Carr III, 1989; Carr III & Elsberry, 1997; Fang & Zhang, 2012; Fiorino & Elsberry, 1989; Moon, Park, & Cha, 2021; Moon, Park, Cha, et al., 2021; Park et al., 2020; Yamada et al., 2016) or suffer different life stages (i.e., developing–mature–decaying stage) during the forecast hours (Elsberry et al., 2007; Huang et al., 2021; Li et al., 2012). Thus, there is a need to find the causes affecting short-term TC forecast and examine the forecast performances of various typhoon cases using numerical weather prediction (NWP) models. Several studies have revealed that TC forecast performances with respect to track, intensity, rainfall, and inner core structure are highly sensitive to the choice of physics parameterization scheme (Biswas et al., 2014; Braun & Tao, 2000; Fovell & Su, 2007; Lord et al., 1984; Shepherd & Walsh, 2017; Smith & Thomsen, 2010; Sun et al., 2014; Wang, 2002; Zhu & Zhang, 2006). Among them, the convective parameterization scheme (CPS), which is directly related to the convective process and precipitation formation, and the cloud microphysics parameterization scheme (MPS), which describes the formation and growth of various water substance variables in the cloud, can significantly affect typhoon forecasts.

Sun et al. (2014) investigated the sensitivity of two CPSs on the simulation of typhoon Megi (2010) using the WRF model with a 20 km horizontal resolution domain and 160 (north–south) \times 180 (east–west) grid points. In their study, owing to the stratiform precipitation of the storm and strong anvil showers from the CPS, the western North Pacific Subtropical High (WNPSH) weakened and large-scale steering flow became anomalously northward, leading to an unrealistic early recurvature of Megi. This mechanism made different typhoon tracks by changing the simulated typhoon structure and its surrounding environment. Shepherd and Walsh (2017) also showed the effect of CPS choice on the simulated tracks of three intense TCs, using the WRF model with a one-way and triply nested (12/4/1.33 km) domain. They found that the sensitivity of the TC track to initial conditions (i.e., initialization time and model domain size) was less than the sensitivity of TC track to changing the CPS. Biswas et al. (2014) conducted comprehensive runs for more than 250 TCs in the Atlantic and Eastern North Pacific basins using the HWRF model with similar configuration to their 2012 operational system (two-way interactive, triply nested domain with 27/9/3 km horizontal grid spacing, and move along with the storm). They found that track and intensity forecasts were highly sensitive to the choice of CPS, which had a significant influence on the resolved-scale scheme in the innermost domain, since the outer domain provides lateral boundary conditions to the inner nested domain.

Wang (2002) conducted a series of sensitivity simulations with idealized initial conditions to evaluate the effects of varying cloud microphysics processes on TCs using the tropical cyclone model (TCM3). The results showed that the cloud structures, along with the peak intensity and area coverage in precipitation in the simulated TCs were changed markedly when different cloud physics processes were included. Zhu and Zhang (2006) also examined the effect of various cloud microphysics processes on the intensity change, precipitation, and inner-core structures of hurricane Bonnie (1998) using the cloud-resolving fifth-generation Pennsylvania State University–National Center for Atmospheric Research (PSU–NCAR) Mesoscale Model (Dudhia, 1993; Grell et al., 1994) with a two-way interactive, triply nested (36/12/4 km) domain. They suggested that the model-simulated hurricane track exhibits little sensitivity to varying cloud physical processes, except for the weakest and shallowest storms. Differences in the cloud microphysical processes significantly affected model-simulated hurricane intensity, inner core structure, and associated cloud and precipitation. In contrast to previous studies, Fovell and Su (2007) found significant track sensitivity to MPSs at operational resolutions (30 and 12 km). In their study, microphysics appeared to directly or indirectly influencing the depth, radial structure, and azimuthal asymmetry of the storm, which could modulate storm motion. Furthermore, recent study of Park et al. (2020) examined the sensitivity of two MPSs on rapidly intensified western North Pacific (WNP) typhoons with westerly movement in low latitudes and poleward movement in the subtropics using a high-resolution (18/6/2 km) WRF model. They found that simulated typhoon intensity and inner core structure were sensitive to the MPSs owing to the distinct hydro-meteor species and their distributions with the schemes. In addition, for poleward moving typhoons, simulated tracks were sensitive to MPSs. They examined the effect of typhoon intensity difference on simulated typhoon size, and therefore on typhoon motion, by comparing the f - and beta-plane experiment. They emphasized that a sophisticated MPS is necessary to improve mid-latitude typhoon forecast performance.

These previous studies have demonstrated that physical parameterization schemes in NWP models can influence the accuracy of TC forecasting. Most of them identified optimal combinations of physics parametrization schemes for small numbers of particular TC cases in their model setting. Thus, it seems necessary to find the

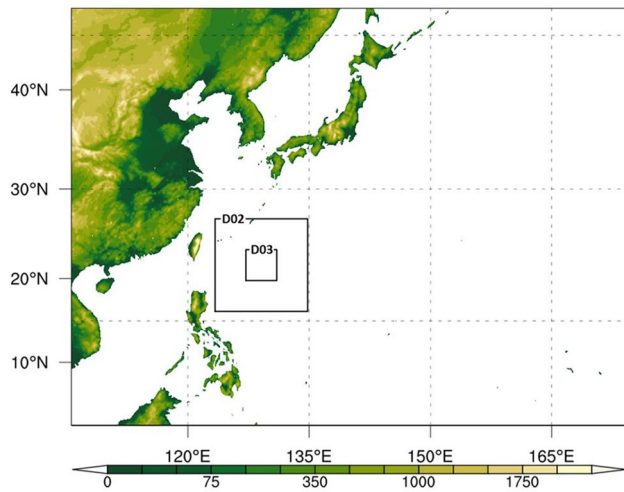


Figure 1. Terrain height (m, shading) and model domains for all the simulations.

optimal physics parameterization schemes for each model to improve the forecast performances of interested typhoon cases using the regional model. We conducted a research collaborating with the Republic of Korea Air Force (ROKAF) recently. Due to the increasing computational resources, the ROKAF's need for the development of a high-resolution operational typhoon forecasting model was increased. Thus, we developed a high-resolution real-time short-term prediction system for forecasting typhoons that would directly/indirectly affect South Korea. As this study was part of the task of developing/improving the newly developed typhoon forecast system, the goal of this study was to investigate the impact of varying CPS and MPS on the real-time short-term forecasts for the recent typhoon cases that affected South Korea and explain the reason for the largest error in typhoon forecast among them. In this regard, we modified one of a scheme followed by Fonseca et al. (2015) and conducted several experiments with it. Those will be done through a series of high-resolution simulations using a two-way interactive, triply nested (12/4/1.33 km), and vortex following WRF model.

The rest of this paper is organized as follows. Section 2 briefly describes the model configuration and experimental design of the sensitivity simulations. The simulation results are presented in Section 3. Section 4 concludes the study.

2. Model Configuration and Experimental Design

WRF model (Skamarock et al., 2019) version 4.1.2 was used for the newly developed typhoon forecast system. We conducted real-time and retrospective runs by using the $0.5^\circ \times 0.5^\circ$ forecast data of National Centers for Environmental Prediction (NCEP) Global Forecasting System (GFS) for the initial and boundary conditions. The model consists of three domains, including one parent domain and two movable nests with 12 km (601×451), 4 km (301×301), and 1.33 km (301×301) horizontal resolutions (grid points), respectively (Figure 1).

We fixed the outermost domain which covers large area enough to forecast various TCs in northern Pacific basin. Also, we used the two-way moving nesting technique for inner two domains. Both domains automatically moved following the typhoon center to resolve the inner core of the typhoon. The model has 35 vertical levels from the surface to the top of the atmosphere at 50 hPa. The integration time steps of the model for domains 1, 2, and 3 were 60, 20, and 6 s, respectively. The model utilized the Yonsei University planetary boundary layer scheme (Hong et al., 2006; Noh et al., 2003), the rapid radiative transfer model for long-wave radiation scheme (Mlawer et al., 1997), and the Dudhia short-wave radiation scheme (Dudhia, 1989). Together, we tested three CPSs—Kain–Fritsch (KF; Kain, 2004), Betts–Miller–Janjić (BMJ; Betts & Miller, 1986; Janjić, 1994), and Modified Tiedtke (TDK; Tiedtke, 1989; Zhang et al., 2011)—and two MPSs—6 class WRF single moment microphysics (WSM6; Hong & Lim, 2006), and Predicted Particle Properties 1-category (P3; Morrison et al., 2015). The CPSs were only employed for convective processes in parent domain with 12 km resolution.

We selected the widely used CPSs and MPSs in real-time global or regional models in our study area. The KF and TDK schemes are somewhat similar in terms of complexity; both are mass-flux type parameterization schemes with updrafts, downdrafts, entrainment, and detrainment of cloud, ice, and snow. Moreover, both use convective available potential energy removal time-scale closure. In contrast, BMJ is one of a profile adjustment schemes that is relaxed toward pre-defined reference temperature/moisture profiles (Arakawa, 2004), without explicit updraft, downdraft, or cloud entrainment of mass flux. The WSM6 considers three additional prognostic hydrometeors (i.e., snow, ice, and graupel), and includes complicated processes via the phase changes among them. The P3 scheme is based on a conceptually different approach to parameterize ice-phase microphysics. All ice-phase hydrometeors are represented by a free frozen category, each of which can represent any type of ice-phase particle. The particles can evolve smoothly in time and space, so that there being the removal of the arbitrary and artificial conversion between categories (Morrison et al., 2015). All other physics schemes and model settings were the same among the sensitivity experiments. Hereafter, we will mention each run as follows, KF_W6 (KF with WSM6), KF_P3 (KF with P3), TDK_W6 (TDK with WSM6), TDK_P3 (TDK with P3),

Table 1
Initial Times and Landfall/Death Date for the Simulated 6 Typhoons

TC number	TC name	Initial forecast time (UTC)	Landfall/Death date (UTC)
1707	Noru	2017/08/03/1200, 2017/08/04 0000, 2017/08/04 1200	2017/08/07 0000
1828	Trami	2018/09/26 1200, 2018/09/27 0000, 2018/09/27 1200	2018/09/30 1200
1830	Kong-rey	2018/10/02 1200, 2018/10/03 0000, 2018/10/03 1200	2018/10/06 0000
1914	Faxai	2019/09/05 1200, 2019/09/06 0000, 2019/09/06 1200	2019/09/09 0000
1915	Lingling	2019/09/03 1200, 2019/09/04 0000, 2019/09/04 1200	2019/09/07 1200
1918	Tapha	2019/09/19 1200, 2019/09/20 0000, 2019/09/20 1200	2019/09/23 0000

BMJ_W6 (BMJ with WSM6), BMJ_P3 (BMJ with P3), modified BMJ_W6 (modified BMJ with WSM6), and modified BMJ_P3 (modified BMJ with P3).

The typhoons that made landfall or directly/indirectly affected the South Korean Peninsula from 2017 to 2019 were selected for our sensitivity experiment. The initial forecast times for each typhoon were set to approximately 3 days before making landfall or when approaching very close to the coastal region. Furthermore, to make general conclusions with respect to landfalling typhoons, we repeated the same simulations but initialized ± 12 -hr from its forecast initial time. Thus, for each combination of CPS and MPS, a total of 18 simulations for six typhoon cases were conducted. The numbers, names, and initial forecast times for each typhoon case are summarized in Table 1.

3. Results

3.1. Sensitivity Experiments With Multiple Physics Schemes

Differences in typhoon track and intensity forecasts among the sensitivity experiments were analyzed by calculating the forecast errors with respect to the best track data (BST) from the Joint Typhoon Warning Center (JTWC). Following Park et al. (2020), the track forecast error was defined as the great-circle distance between the center position of a typhoon forecast and the best track position. Intensity forecast error is defined as the difference between the intensity forecast (i.e., maximum 10-m wind speed, MWS; minimum sea-level pressure, MSLP) and best track intensity at the forecast hour. Furthermore, to investigate the difference in speed and direction between the typhoon forecast and best track position, we analyzed the cross-track bias and along-track bias of all sensitivity experiments. The cross-track error is defined as the component of absolute error in the direction perpendicular to the best track of the typhoon. Also, along-track error is defined as the component of absolute error in the direction of the best track of the typhoon (Chen et al., 2015). Similarly, the cross- and along-track bias (CTB and ATB) are based on the concept of transition direction and velocity of the typhoon. Thus, positive values of CTB indicate a simulated typhoon track that is located to the right side of the best track. And positive values of ATB indicate a simulated typhoon that moves faster than the best track.

To identify differences in typhoon forecast performances among all sensitivity experiments, we compared the average track and intensity errors, CTB, and ATB in 24-hr intervals (Figure 2). Generally, both the typhoon track and intensity forecast performances are improved significantly in KF_W6, while BMJ-applied runs, such as BMJ_W6 and BMJ_P3, show the worst track forecast performances (Figures 2a and 2b). P3-applied runs markedly overestimated simulated typhoon intensities, especially in the intensification period (48-hr). It is noteworthy that significantly strong negative CTBs occurred in BMJ- and P3-applied runs from the mid-to late forecast hours (48–72 hr; Figure 2c). In particular, the maximum difference between the BMJ-applied runs and the others at 72-hr was more twofold. Similar to the CTB trends, the strong negative ATBs occurred in the same runs (Figure 2d). These results indicate that BMJ- and P3-applied runs tended to simulate westward and slowly moving typhoons compared with the JTWC BST and other sensitivity experiments.

Figures 3 and 4 show the 3-day track and intensity forecast results for two representative typhoons with their maximum CTB and ATB at each forecast hour (track and intensity forecast results for other typhoon cases, see Figures S1–S4 in Supporting Information S1). Faxai (2019) has a relatively small track forecast error and track spreads; Trami (2018) has large track forecast errors and track spreads. Here, the track spreads are represented by the maximum CTB and ATB among all sensitivity experiments. BMJ- and P3-applied runs tended to simulate

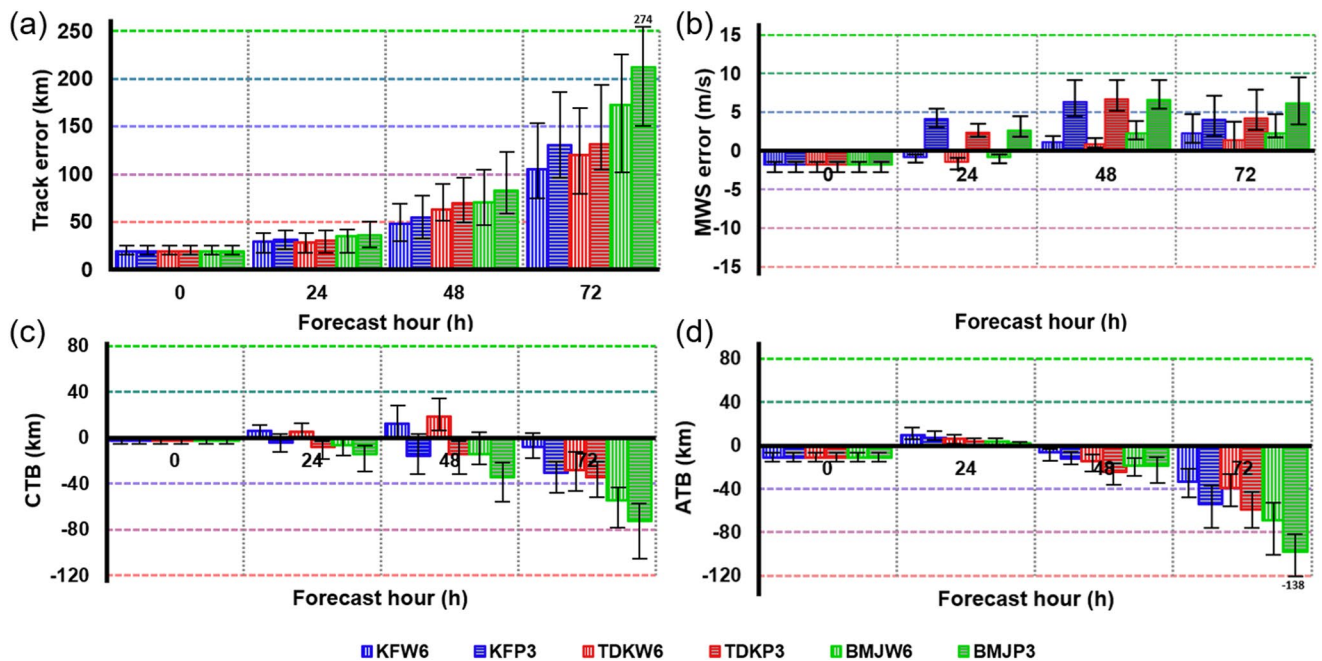


Figure 2. Mean forecast (a) track error (km), (b) maximum 10-m wind speed (MWS) error (m s^{-1}), (c) cross-track bias (CTB; km), and (d) along-track bias (ATB; km) of the 0-, 24-, 48-, 72-hr forecasts in all sensitivity experiments. Blue: Kain–Fritsch (KF); red: Modified Tiedtke (TDK); green: Betts–Miller–Janjić (BMJ). Vertical shading: six class WRF single moment microphysics (WSM6); horizontal shading: Predicted Particle Properties 1-category (P3). Error bars represent the spread between the 25th and 75th percentiles.

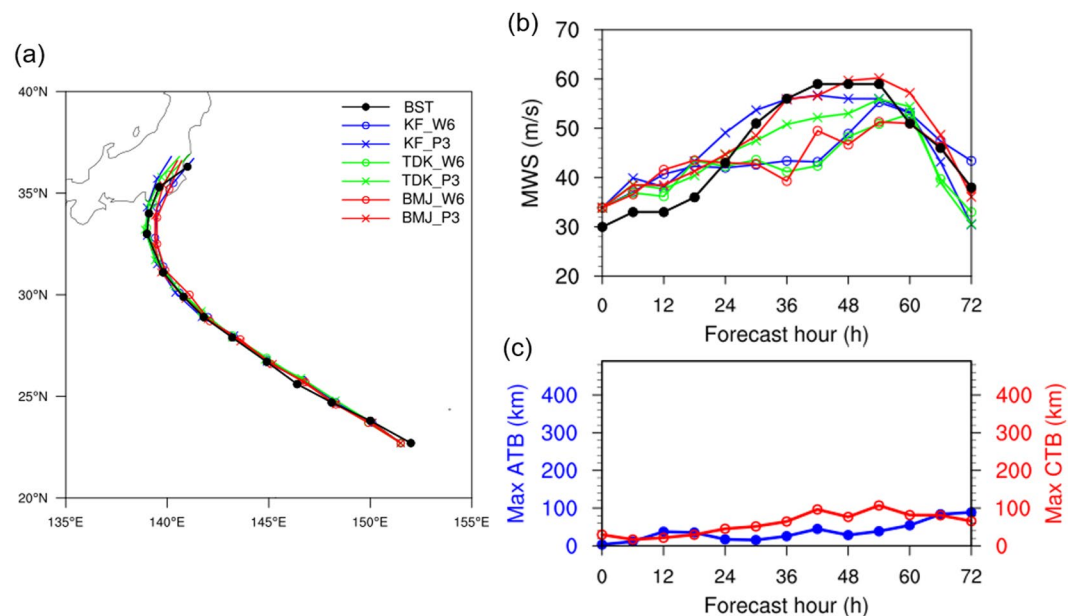


Figure 3. Simulated (a) track and (b) maximum 10-m wind speed (MWS; m s^{-1}) for all simulations and the Joint Typhoon Warning Center (JTWC) best track data (BST; black). Blue: Kain–Fritsch (KF); red: Modified Tiedtke (TDK); green: Betts–Miller–Janjić (BMJ); Circle: 6 class Weather Research and Forecasting (WRF) single moment microphysics (WSM6); cross: Predicted Particle Properties 1-category (P3). (c) Maximum track spread (km) in the along and cross directions (ATB and CTB, respectively) among all sensitivity experiments at 6-hr intervals for typhoon Faxai (initialized at 0000 UTC 06 Sep 2019).

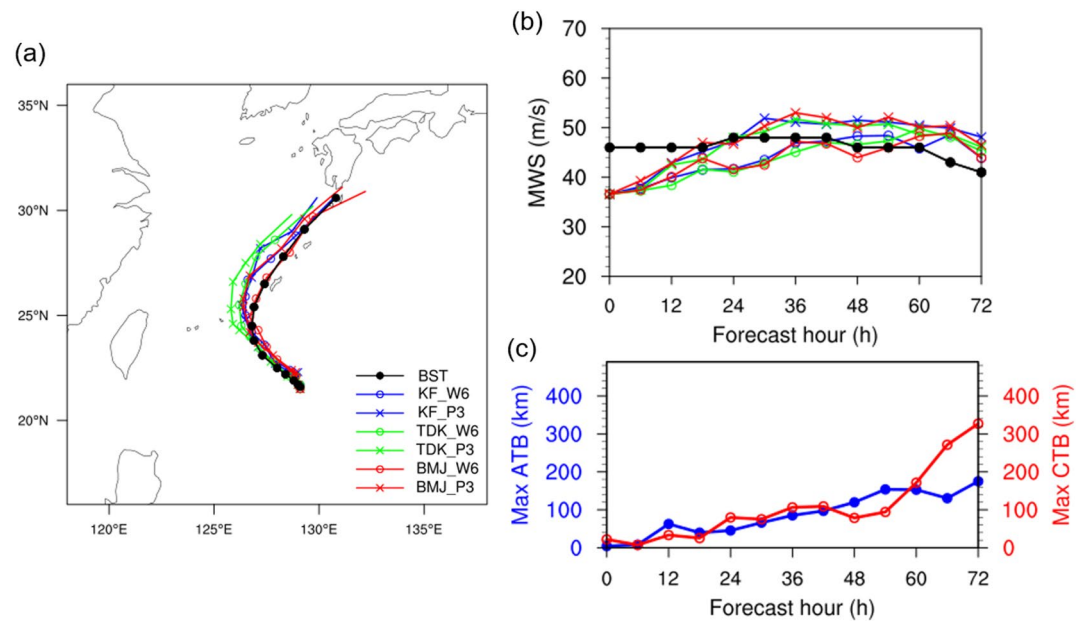


Figure 4. Same as Figure 3 but for typhoon Trami (initialized at 0000 UTC 27 Sep 2018).

more westward and slowly moving typhoons (Figures 2c, 3a and 4a). Furthermore, typhoons simulated in the P3-applied runs were the strongest, and more rapidly intensified than the WSM6-applied runs (Figures 3 and 4b). All sensitivity experiments produced relatively small track spreads (<150 km) for typhoons Kong-rey, Lingling, and Faxai (Figure 3c), and large track spreads (>350 km) for typhoons Noru, Trami, and Tapha (Figure 4c). The simulated results did not change significantly when we changed typhoons' initial forecast times. In the case of a relatively small track spread, the track spreads slightly increased just before the end of the forecast. However, the track spreads rapidly increase from the early or mid- (after 24- or 48-hr) forecast hours in the large spread cases, most of which are contributed by the westward-moving typhoons in BMJ-applied runs and relatively eastward-moving typhoons in KF- and TDK-applied runs (e.g., typhoon Trami, Figure 4a). In addition, there were relatively small track spreads between the applied MPSs. Nevertheless, slightly westward-moving typhoons were simulated in P3-applied runs, related to the simulated intensity of typhoons as mentioned before. All typhoon cases, even with small track spreads (e.g., Kong-rey, Lingling, and Faxai), have similar characteristics of track forecast that the track spreads among the MPSs are much smaller than that of the CPSs. Those results indicate that CPS can have a much greater impact on typhoon track forecast than MPS.

To explain the reasons for the different track spreads among the sensitivity experiments for two cases, we compared their simulated large-scale environmental fields. Figures 5 and 6 show the mid-level (500 hPa) synoptic fields, variance/average of GPH among the CPSs, MPSs, and total GPH variance/average during the 24–48 hr forecasts of typhoon cases Faxai and Trami in all sensitivity experiments. The representative middle-level GPH line is defined by the 5,890 gpm contour, which depicts Z_{500} as the approximate size of the WNPSH. Overall, the simulated WNPSH in KF- (Figures 5a and 5b and 6a–6b) and TDK-applied runs (Figures 5c and 5d and 6c–6d) was relatively strong and expanded southwestward compared with the BMJ-applied runs (Figures 5e and 5f and 6e–6f). It is noteworthy that when the WNPSH was relatively contracted northeastward, the track spreads were small (e.g., typhoon Faxai; Figures 3a and 5, and Figure S5a in Supporting Information S1). In contrast, when the WNPSH was relatively expanded further southwestward, the track spreads of simulated typhoons were large (e.g., typhoon Trami; Figures 4a and 6, and Figure S5b in Supporting Information S1). In addition, several regions showed large variance among CPSs mainly located below 20°N in both cases (bottom panels in Figures 5 and 6). The variance in GPH around the WNPSH was only large in the Trami case, implying the differently simulated WNPSH among the CPSs. Relatively low GPH values at low latitudes in BMJ-applied runs are in agreement with the large variance regions among the CPSs. In both typhoon cases, the GPH variance was considerably large in the vicinity of typhoon (righthand panels in Figures 5 and 6). These results suggest that the sensitivity of typhoon track forecast performance to the physical model settings might not be quite large when the WNPSH is contracted and shifted northeastward. Moreover, the large track spread among the CPSs could be caused by the

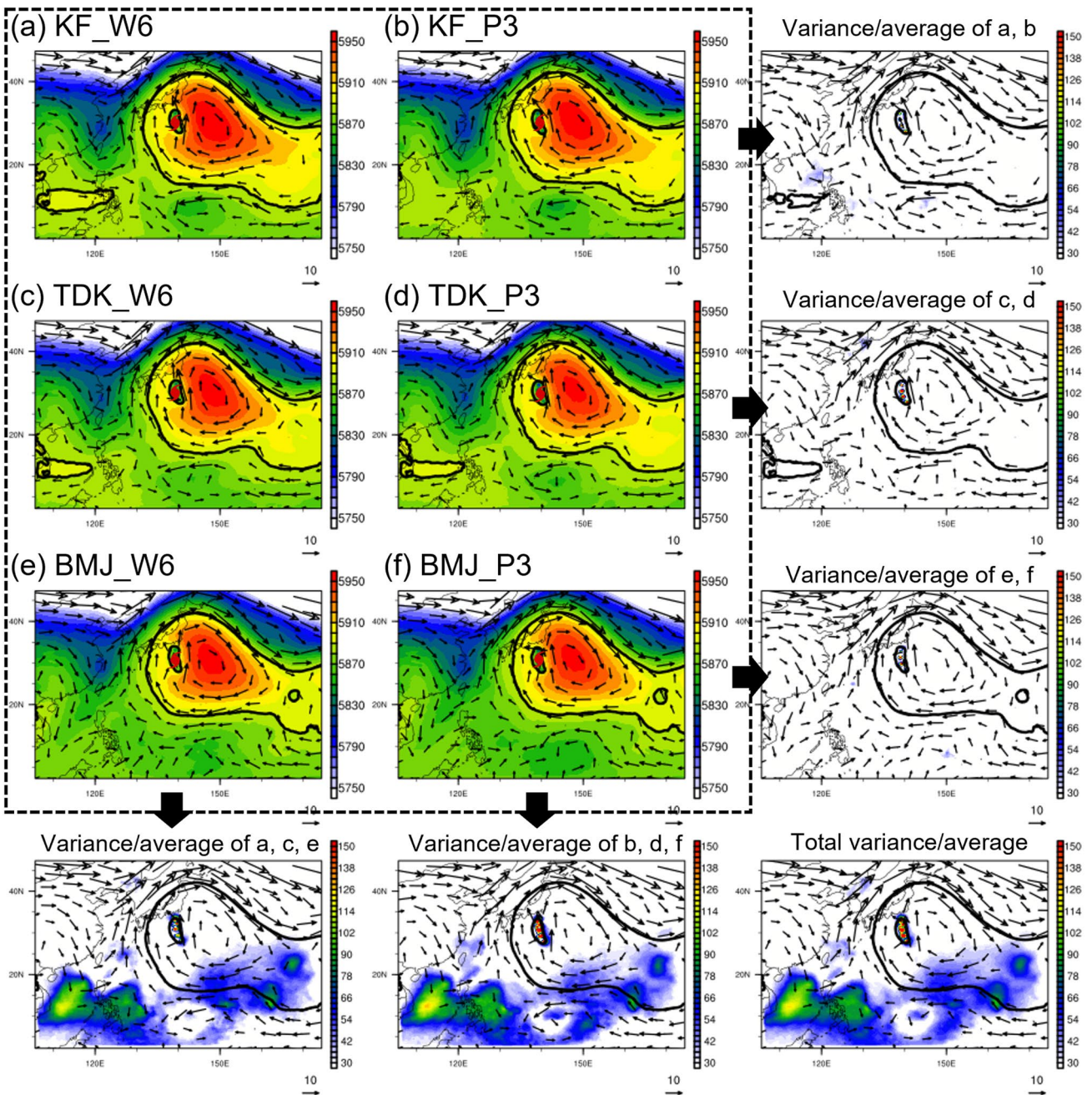


Figure 5. Simulated geopotential height (GPH; gpm, shading) and wind fields (m s^{-1} , vector) at 500 hPa during the 24–48 hr forecast for typhoon Faxai (initialized at 0000 UTC 06 Sep 2019) in the 12 km domain. Contour lines are the 5,890 GPH (gpm) line (Z_{500} ; gpm, contour). The rightmost column and bottom row show the GPH variance (shading) and average (contour) of different groups of simulations. Red marks represent mean typhoon location.

expansion or contraction of the simulated WNPSH. There are large variance regions between the MPSs near the typhoons because the choice of MPS can affect the simulated typhoon intensity and structure. Also, the variance at higher latitudes was not notably large, implying no significant differences in the simulated mid-latitude trough or jet stream among the sensitivity experiments. This might be related to our fixed parent domain; the WNPSH and trough are simulated at the parent domain's interior and boundary, respectively, resulting in relatively small and large differences for the mid-latitude trough and WNPSH among all the sensitivity experiments.

Figure 7 shows the simulated low-level (850 hPa) horizontal wind structure, distribution of 6-hr accumulated precipitation, azimuthally averaged tangential/radial wind fields, and temperature anomaly of typhoon Trami at

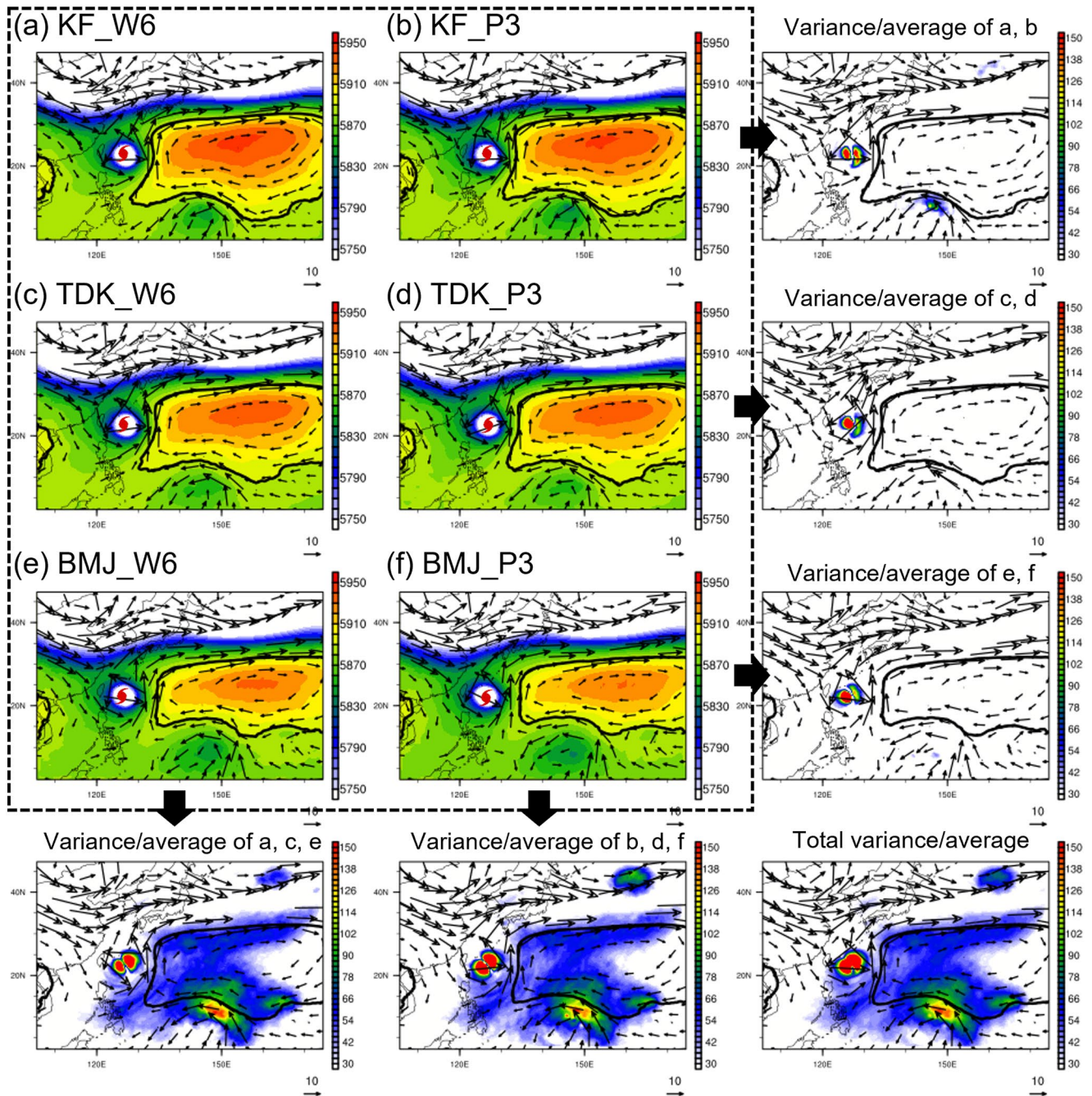


Figure 6. Same as Figure 5 but for typhoon Trami (initialized at 0000 UTC 27 Sep 2018).

1200 UTC 28 Sep 2018 in KF_W6 and KF_P3. They are analyzed here to compare the impacts of MPSs on the horizontal and vertical structures of the typhoon forecasts during their lifetime maximum intensity period. The results show that the strongest low-level wind field (Figure 7a), the heaviest surface precipitation (Figure 7b), the largest storm size, the most robust secondary circulation (Figure 7c), and the strongest warm-core structure (Figure 7d), all of which are related to more destructive features of the typhoon structure, were simulated in sensitivity experiment with P3 scheme. Those results indicate that the westward bias of typhoon tracks (Figures 2c, 3a and 4a) in the P3-applied runs seems to be related to the beta effect, causing more extensive and powerful TCs to move northwestward in the northern hemisphere (Park et al., 2020). Simulated typhoon structures tend to be more symmetric from the low-to upper-levels with increasing typhoon intensity. In addition,

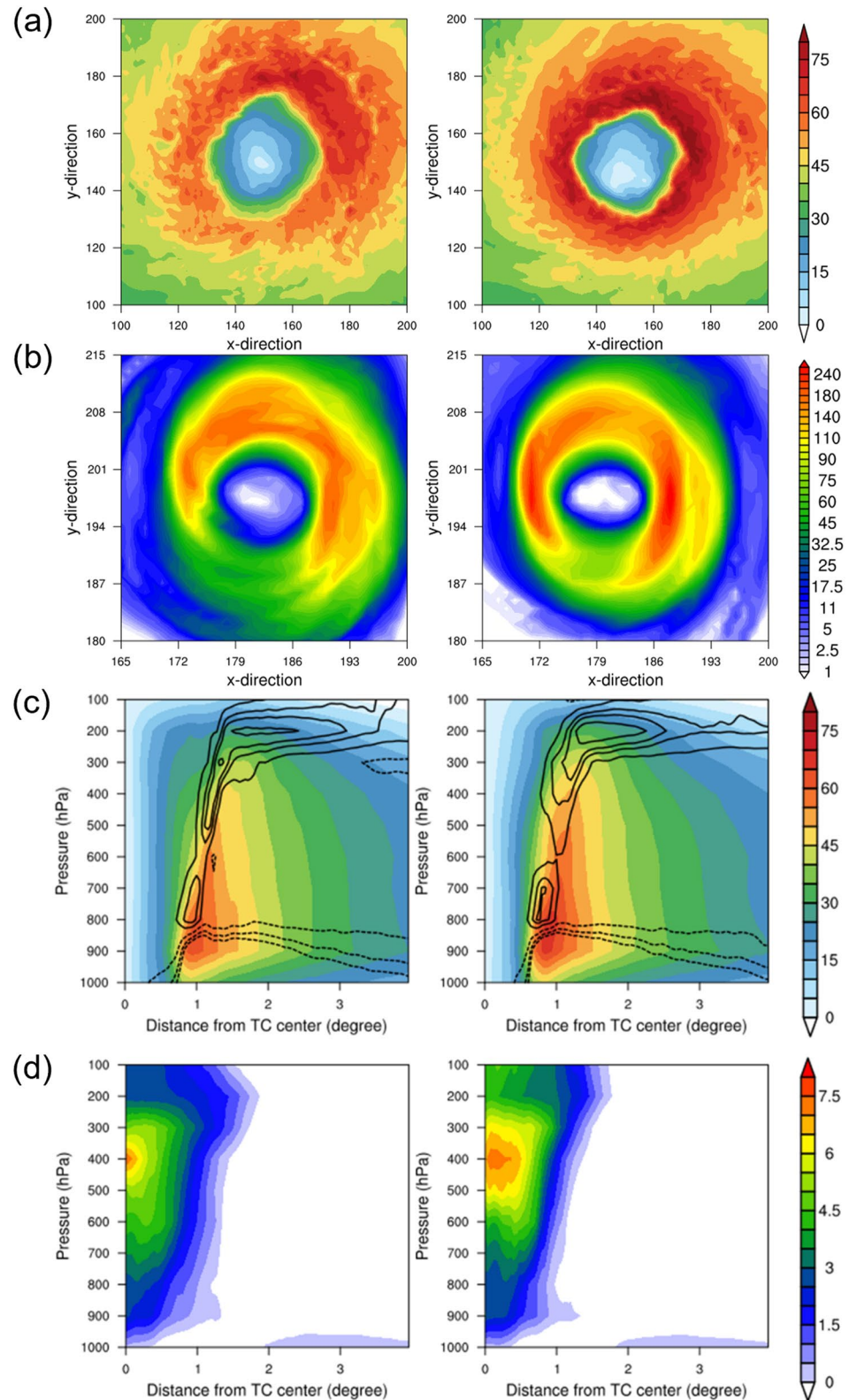


Figure 7. Horizontal structure of simulated (a) wind speed (m s^{-1}) at 850 hPa, (b) 6-hr accumulated precipitation (mm), vertical and radial structure of azimuthal mean of (c) tangential (m s^{-1} , shading) and radial (m s^{-1} , contour) wind, and (d) temperature anomaly (K) in KF_W6 (left) and KF_P3 (right) simulations in the 4 km domain at 1200 UTC 28 Sep 2018 for typhoon Trami (initialized at 0000 UTC 27 Sep 2018). The radial wind is shown with intervals of 3 m s^{-1} .

simulated typhoon structures with the WSM6 scheme were similar to those from satellite data and similar to the radius estimates of four quadrants of the typhoon from the JTWC BST data, which showed asymmetric structures overall (not shown).

In succession to the previous results, the enormous microphysical latent heating is simulated in KF_P3 (not shown). In general, microphysics processes such as liquid condensation inside the eyewall and deposition, accretion, and freezing of frozen particles in the upper layer generate latent heat. And a large amount of latent heat in the eyewall region affects the expansion of the atmospheric column, leading to a pressure drop at the surface and finally causing strengthened typhoons and stronger amounts of precipitation. Thus, previous results indicate the different microphysical processes included in each MPS cause significant differences in simulated typhoon structure. As aforementioned before, the WSM6 scheme has complex microphysical processes. WSM6 allows the existence of supercooled water, and so processes such as snow growth by riming ice crystals or forming graupel by riming of snow are included in the scheme (Hong & Lim, 2006). Furthermore, it also considers graupel, solid-type hydrometeors, and related microphysical processes. However, unlike the traditional MPSs, the P3 scheme does not categorize the ice-phase hydrometeors (i.e., ice, snow, hail, graupel) according to their densities or sizes. Instead, it prognoses ice-phase hydrometeors using a single category, which allows diverse ice-phase particles to be present in the same grid box and time (Morrison et al., 2015). In this regard, a variety of ice-phase hydrometeors remains uncertain, but they could evolve ice to a state with any set of properties (i.e., snow, hail, graupel). Thus, to further investigate their different influences on typhoon intensity or structure forecast, we compared the distribution of horizontally and azimuthally averaged microphysical hydrometeors simulated in KF_W6 and KF_P3 for typhoon Trami (Figure 8). The result showed that from the initial forecast time (6-hr forecast), the enormous amount of ice and cloud water mixing ratios were distributed more widely and highly in the P3-applied run. In addition, the result was consistent after the initial forecast time, and these differences were much more significant when the intensity difference between the two runs was larger. It seemed that the highly distributed cloud ice (up to 150 hPa) had a strong impact on the widespread distribution of ice mixing ratio in the P3-applied run (Figure 8d). It is known that at temperatures between 0°C and −40°C most clouds contain a mixture of ice crystals and supercooled water droplets. It seemed that the coexistence of cloud water and cloud ice mixing ratios distributed from 0°C to −40°C was more significant in the P3-applied run, and they could act like supercooled water. Thus, the formation of cloud ice might also be enhanced in the P3-applied run.

For further analysis of the cloud microphysical processes in the inner cloud, we additionally conducted 6-hr simulations for typhoon Trami with 10-min output interval and analyzed the area-averaged and vertically integrated microphysical processes in the two schemes (see Figures S7 and S8 in Supporting Information S1). The results showed that stronger vapor condensation processes occurred in the P3 scheme, implying that a larger amount of cloud water was produced. In addition, it is known that the deposition (gas to solid) process releases more amount of latent heat than the accretion (liquid to solid) process. However, the graupel accretion was the most prominent process in the WSM6 scheme, which means that the production of graupel by the accretion process was the most important contributor to the upper layer latent heat in the WSM6 scheme (see Figures S7 and S9 in Supporting Information S1). On the other hand, the ice deposition was the strongest processes in the P3 scheme, implying that the production of the ice by the deposition was the most important contributor to the upper layer latent heat in that scheme (see Figures S8 and S12 in Supporting Information S1). The underlying cause of all these results was related basically different concepts of parameterized ice-phase microphysics. Since the ice could be instantly converted into snow and graupel, the graupel and snow accretion processes were relatively larger than ice deposition process (see Figures S9-S11 in Supporting Information S1). In contrast, the ice deposition process was dominant in the P3 scheme. Thus, latent heat release at the upper level of the P3 scheme was strengthened more by the deposition of ice term, leading to the development of deep convection, and again, the upward motion could be enhanced, resulting in more amount and growth of cloud ice. In summary, why P3 scheme results in always stronger typhoons could be associated with two reasons; more enhanced formation of ice by the abundant amount of supercooled droplets at the higher level by strong upward motion in the P3 scheme, also, deposition of ice was the main process of releasing the latent heat in the upper deep clouds, since there were no more microphysical processes for the conversion of ice to snow or graupel.

To summarize the results, we calculated the track and intensity spreads of all typhoon cases at each forecast hour (Figure 9). Here, the spreads of track and intensity were defined as the maximum difference in distance (km) and MWS (m s^{-1}) for each typhoon, respectively. The results clearly show that typhoon track and intensity spreads are sensitive to the CPSs and MPSs, respectively. In other words, when the same CPS (MPS) is used, the

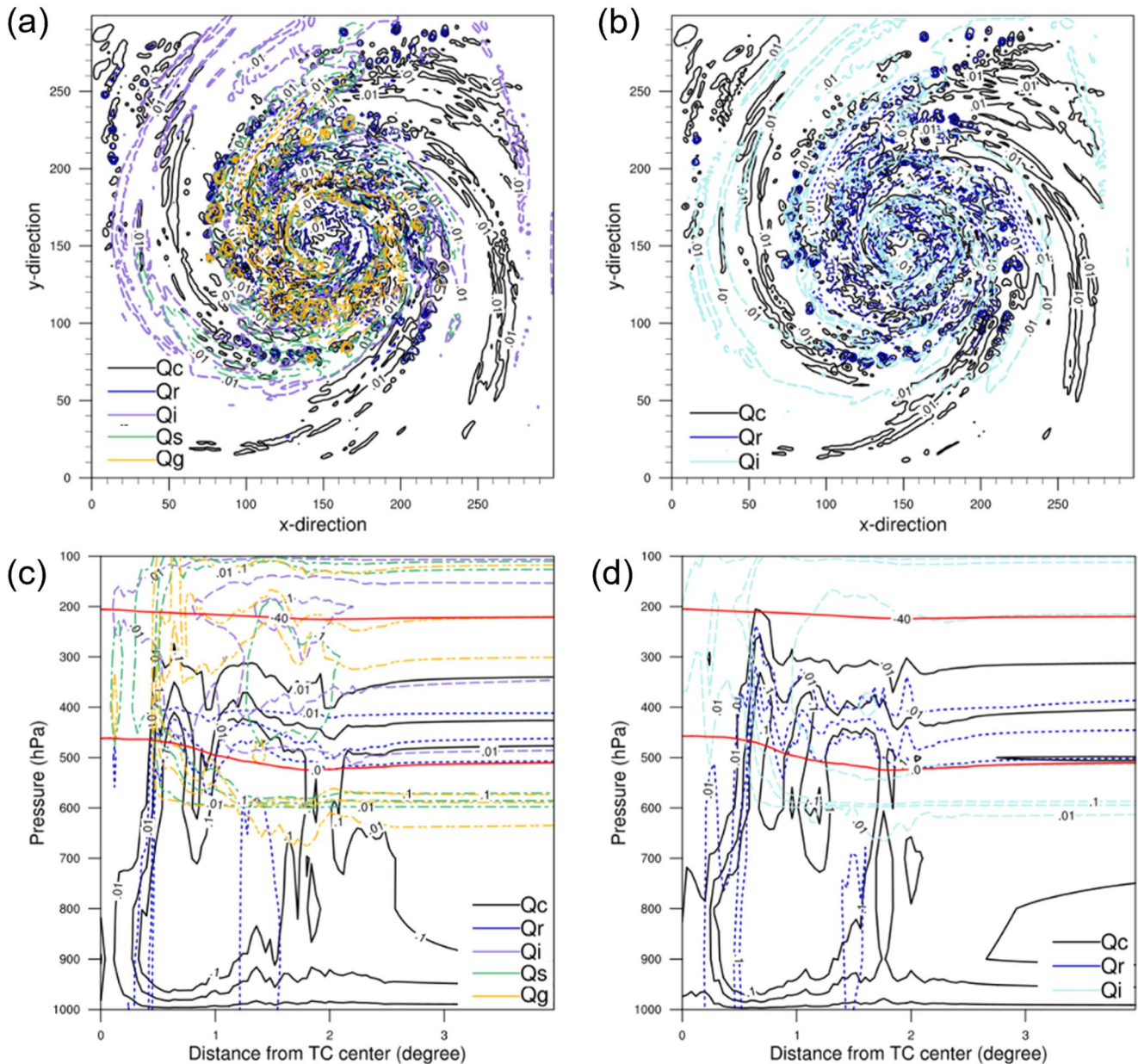


Figure 8. Horizontal structure of vertically integrated microphysical hydrometeors in (a) KF_W6 and (b) KF_P3 simulations and Vertical and radial structure of the azimuthal mean of microphysical hydrometeors in (c) KF_W6 and (d) KF_P3 in the 4 km domain at 0600 UTC 28 Sep 2018 for typhoon Trami (initialized at 0000 UTC 27 Sep 2018). Q_c , Q_r , Q_i , Q_s , and Q_g indicate cloud water, rain water, ice, snow, and graupel, respectively. Contour lines are at 0.01, 0.03, 0.06, 0.15, 0.5, 1.5, 3.0, and 5.0 g kg^{-1} . Contour lines denote the 0°C and -40°C temperature layers, respectively.

typhoon track (intensity) might not be changed significantly by choice of the MPS (CPS). The track spread tends to increase gradually with increasing forecast lead time owing to the growth of dissimilarities in each sensitivity experiment (Figure 9a). On the other hand, increasing or decreasing trends of average intensity spread strongly depend on the selection of typhoon case. Since most cases reached their lifetime maximum intensity around in the middle of the forecast lead time, intensity spread increased until 42-hr forecast time and then decreased after the maximum lifetime intensity (Figure 9b).

Overall, the results were strongly related to model configuration. We used CPSs only for the parent domain, since the two inner nested domains had fine resolutions, and so the different effects of simulated synoptic-scale environmental fields with the various CPSs were shown as the track spread. The choice of MPS largely affected the typhoon intensity and inner core structure forecasts, with the differences shown as the intensity spread. This

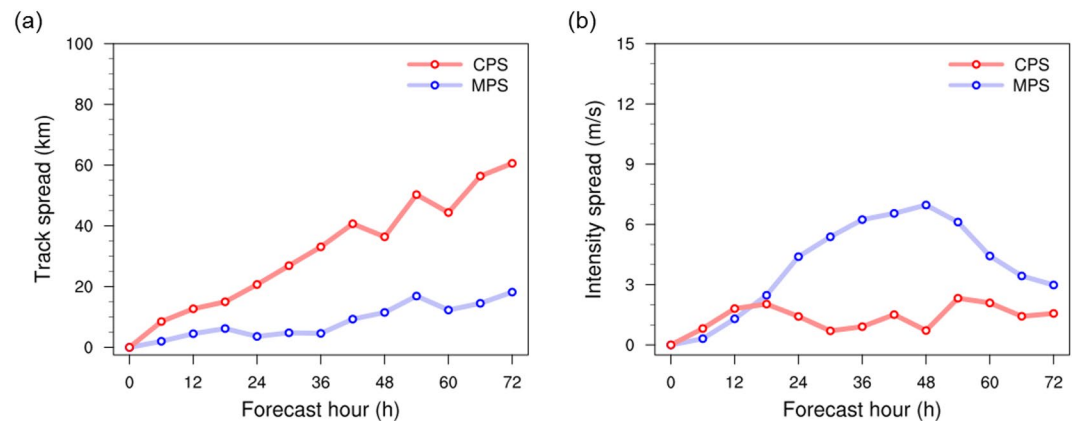


Figure 9. Comparison of (a) track and (b) intensity spreads between the convective parameterization schemes (CPSs) and cloud microphysics parameterization schemes (MPSs) used in this study at each forecast hour for all simulated typhoon cases (blue: MPS, red: CPS).

elucidates why the intensity forecasts were similar for all simulated typhoon cases when the same MPS was applied.

3.2. Sensitivity Experiments With a Modified BMJ Scheme

In this section, we additionally conduct several sensitivity experiments with a modified BMJ scheme to explain the reason for a large track error in the BMJ-applied runs. As shown in Figures 5 and 6, there was a significant GPH variance region among the CPSs at low latitudes, because the large differences of GPH simulated in the BMJ-applied runs. These differences affected the strength and expansion of the simulated WNPSH in the BMJ-applied runs, resulting in larger differences in simulated typhoon tracks during the forecast hours. Thus, it is important to simulate the WNPSH correctly to improve typhoon track forecast performances when the WNPSH is expanded westward, such as in the Trami case. In this regard, we focused on finding the reason for the significant differences in the low latitudes, especially in the BMJ-applied runs. Fonseca et al. (2015) showed that cumulus precipitation is very sensitive to the temperature and humidity reference profiles in the BMJ scheme. They investigated the sensitivity of precipitation produced by the BMJ scheme to changes in two parameters and found that excessive rainfall region around the tropics was significantly decreased when using the modified BMJ scheme. This scheme outperforms the Climate Forecast System Reanalysis (CFSR) for the whole tropics and both monsoon seasons (Fonseca et al., 2015). From their study, we hypothesized that the poorly simulated rainfall in the low latitudes could affect the WNPSH simulation in the BMJ-applied runs. Thus, we modified the two factors related to the temperature and humidity profile in the BMJ scheme (hereafter, Modified BMJ scheme), similar to those in Fonseca et al. (2015) (Table 2). We increased α to make a warmer reference profile and decreased F_s to make a more moist humidity reference profile to generate a smaller amount of cumulus precipitation than the BMJ scheme. We then conducted additional sensitivity experiments with the modified BMJ scheme for all typhoon cases.

Figure 10 compares the average track error (km) and CTB (km) between the BMJ and modified BMJ schemes in 24-hr intervals. Generally, the modified BMJ-applied runs significantly improved the typhoon track forecast performances, especially for the 72-hr results (Figure 10a). The strong negative CTBs and ATBs (not shown) are also notably decreased in the modified BMJ-applied runs (Figure 10b). This means that relatively smaller westward bias and faster typhoons are simulated by the modified BMJ scheme. However, the track errors and CTBs are somewhat still large compared with the best physics combination defined in the previous section. Here, we do

not show the simulated typhoon intensity errors. As we mentioned earlier, in our model setting, CPSs were not activated in the two inner moving domains, which fully cover the typhoons and follow their center points over the simulation hours. It caused that CPSs could not directly affect the typhoon itself, but they could indirectly interact with the inner domain at the boundary of the inner domain. Thus, simulated typhoon intensity performances were not significantly changed among the CPSs even when using the Modified BMJ scheme.

Table 2
Comparison of Two Factors Used in the BMJ and Modified BMJ Sensitivity Experiments

	BMJ	Modified BMJ
α	0.9	1.2
F_s	0.85	0.6

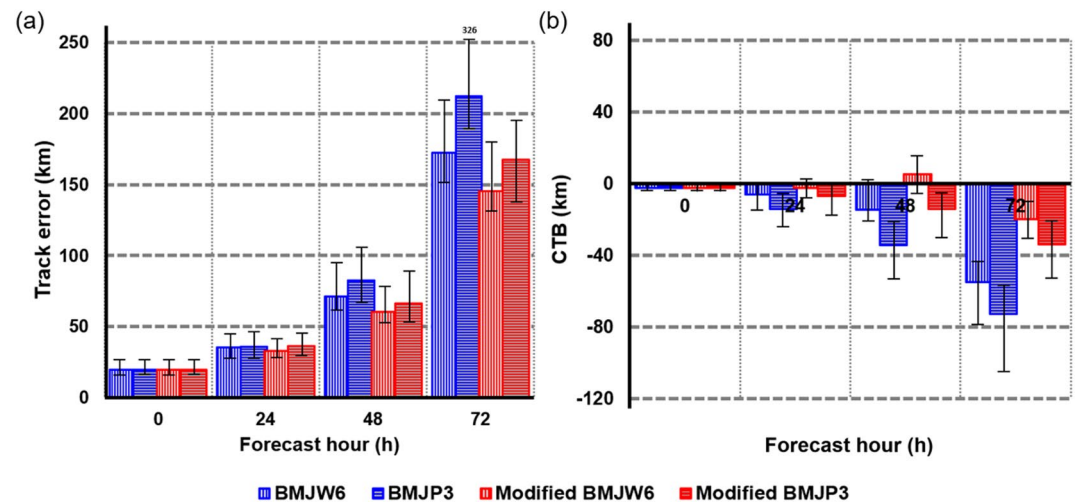


Figure 10. Mean forecast (a) track error (km) and (b) cross-track bias (CTB; km) at the 0-, 24-, 48-, 72-hr forecast in the Betts–Miller–Janjić (BMJ) and modified BMJ sensitivity experiments. Blue: BMJ; red: modified BMJ. Vertical shading: six class WRF single moment microphysics (WSM6); horizontal shading: Predicted Particle Properties 1-category (P3). Error bars represent the spread between the 25th and 75th percentiles.

Figure 11 shows the 3-day track and intensity forecast results of typhoon Trami with modified BMJ scheme, and their maximum track spread at each forecast hour. Typhoon tracks, westward shifted in BMJ-applied runs (Figure 4a), are reasonably simulated in modified BMJ-applied runs (Figure 11a). Similar to the original result (Figure 4b), simulated typhoons in the modified BMJ_P3 are stronger than in modified BMJ_W6 (Figure 11b). Moreover, the track spread decreased by more than 100 km at the 72-hr forecast time when applying the modified BMJ scheme (Figure 11c). These results are consistent with other typhoon cases, such as Noru and Tapha, which already had large track spreads among all sensitivity experiments. Also, the modified BMJ scheme further reduced track spreads for Kongrey, Lingling, and Faxai with relatively small track spread (not shown).

Figure 12 shows the mid-level synoptic fields, variance/average of GPH among the CPSs, MPSs, and total GPH variance/average during the 24–48 hr forecasts of typhoon Trami in the KF-, TDK-, and modified BMJ-applied runs. The most noticeable difference between Figures 6 and 12 is the dramatically decreased GPH variance

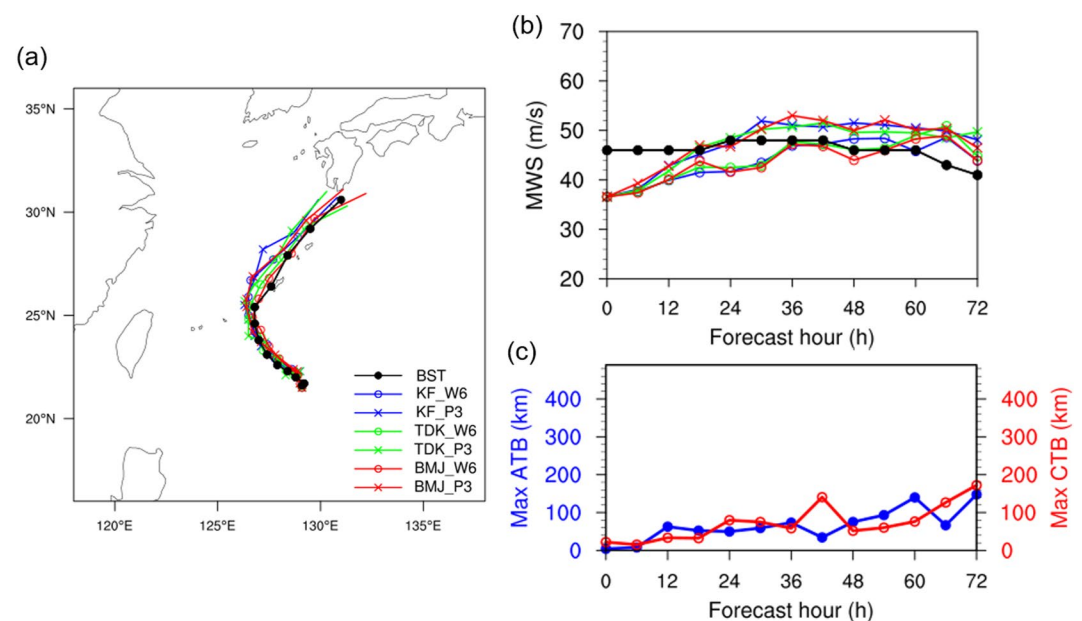


Figure 11. Same as Figure 4 but with the modified BMJ sensitivity experiments.

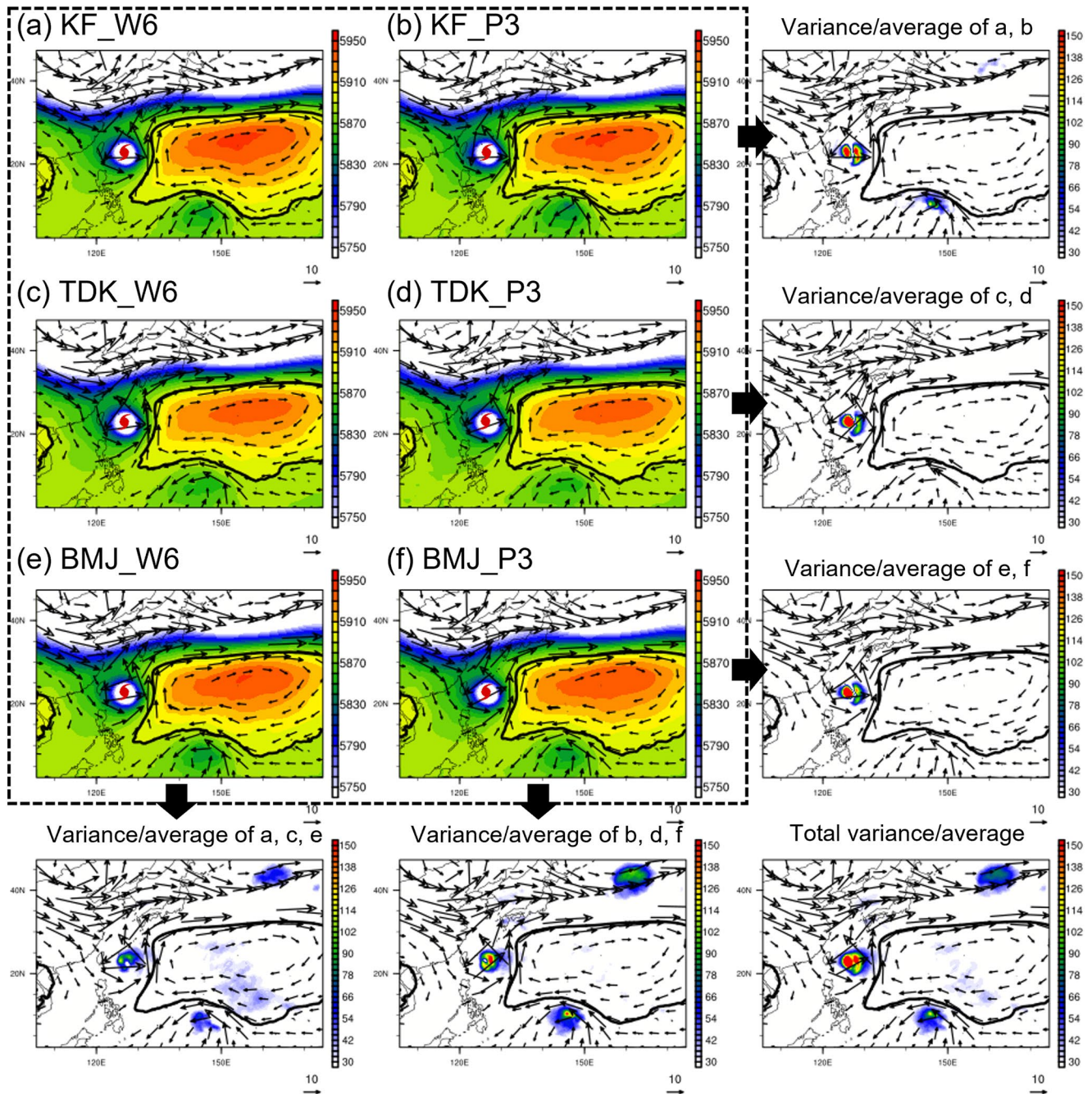


Figure 12. Same as Figure 6 but with the modified BMJ sensitivity experiments.

among CPSs near low latitudes and in the vicinity of typhoons when using the modified BMJ scheme (bottom panels in Figure 12). Simultaneously, the simulated WNPSH by the modified BMJ scheme extended further southwestward, similar to the KF- and TDK-applied runs, and greatly affected the typhoon movement than the original results. To investigate the reason why GPH variance differs between the BMJ- and modified BMJ-applied runs, we analyze each simulation results for the upper and lower tropospheric environments.

Figure 13 shows the simulated synoptic fields in the middle and upper troposphere (500–300 hPa; Figure 13a) and the surface and lower troposphere (1,000–850 hPa; Figure 13b) of BMJ_W6 and modified BMJ_W6. In the case of BMJ_W6, precipitation occurred in a wide area at low latitudes, where convection formed over wide-range and reached the upper troposphere. Convection also existed extensively (around 110°E–120°E) only

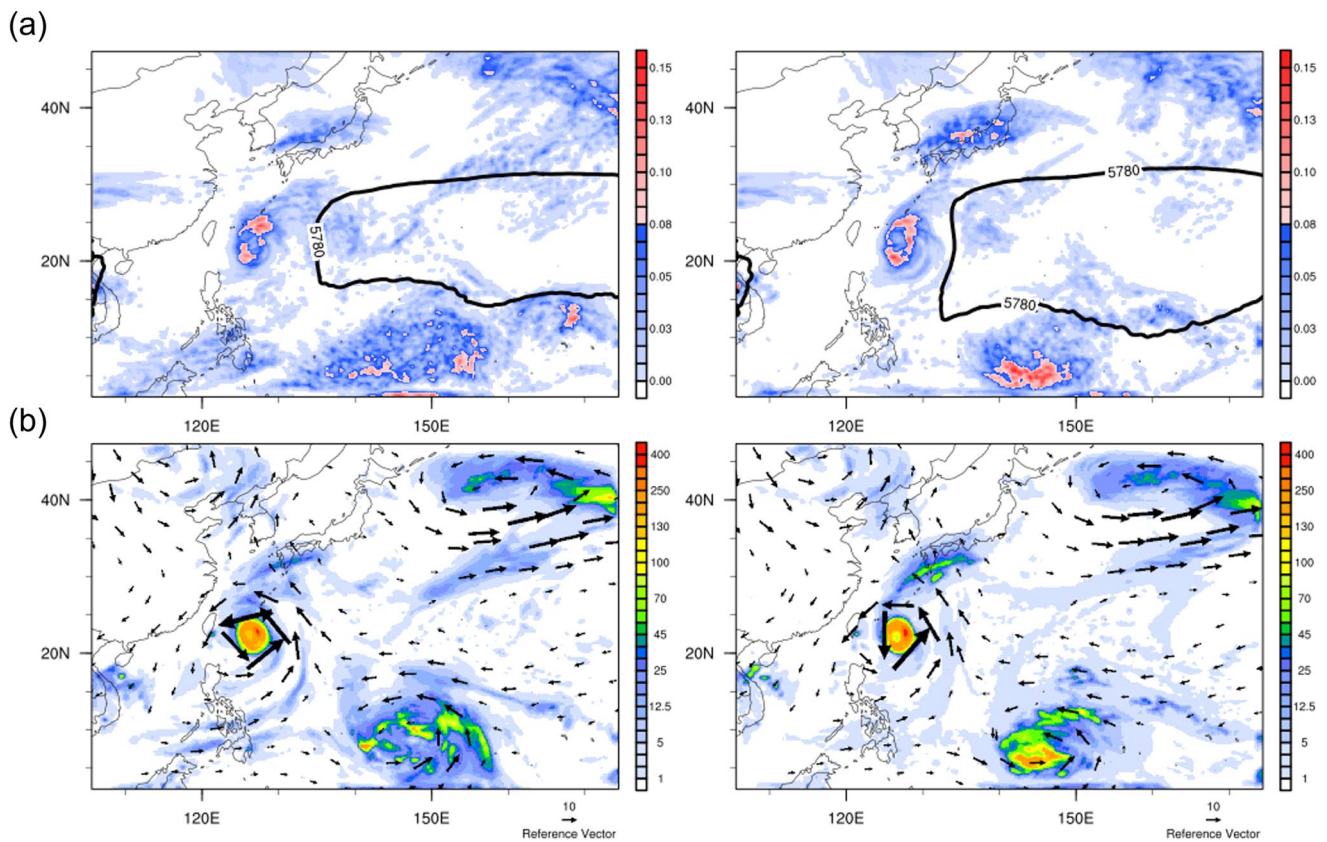


Figure 13. Comparison of simulated (a) mixing ratio of ice (g kg^{-1} , shading) at 300 hPa and GPH line at 500 hPa (Z_{500} : gpm, contour) and (b) 24-hr accumulated precipitation (mm, shading) and wind fields A (m s^{-1} , vector) at 850 hPa in BMJ_W6 (left) and modified BMJ_W6 (right) during the 24–48 hr forecast for typhoon Trami (initialized at 0000 UTC 27 Sep 2018) in the 12 km domain.

in BMJ_W6. Moreover, Z_{500} was contracted owing to excessive CPS-induced shallow precipitation at low latitudes. In contrast, in the modified BMJ_W6, precipitation occurred in a relatively narrow area, resulting in the expansion of strengthened WNPSH. In addition, when compared with IMERG (Integrated Multi-satellite Retrievals for GPM) data, the modified BMJ-applied runs reasonably captured the localized precipitation at low latitudes (not shown).

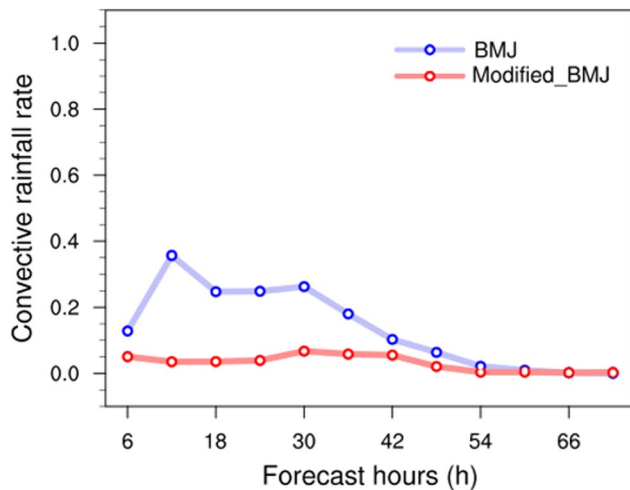


Figure 14. Comparison of averaged convective rainfall rate in the vicinity of typhoons (within a 500 km radius) between the Betts–Miller–Janjić (BMJ)- and modified BMJ sensitivity experiments at 6-hr intervals for all typhoon cases (blue: BMJ, red: modified BMJ).

We also calculated the rate of averaged CPS-induced precipitation within a 500 km radius for all the typhoons at each forecast time to compare the effect of the two adjusted parameters (Figure 14). Because the BMJ scheme is over-activated to remove atmospheric instabilities in the tropics, the impact of reduced CPS activation was most significant at the early forecast hours. In modified BMJ-applied runs, the precipitation ratio by the CPS decreased at the early forecast hours, implying an enlargement of the amount of precipitation by the MPS. Besides, we found that convection, which was associated with another typhoon Kong-rey in the developing stage, was weakly simulated in BMJ-applied run (left figures in Figure 13). This result showed that, when another typhoon was located at the low-latitude region, as in the Trami case, CPS overactivation could weaken the WNPSH as well as prevent the typhoon from developing well. In other words, these results suggest that the typhoons at low-latitude region might not be realistically intensified when using the BMJ scheme with low horizontal resolution, even if the P3 scheme is used for the MPS.

To summarize the previous results, overall forecast performances were improved when using the modified BMJ scheme. The typhoon track forecast

performances were significantly improved, and these results were strongly related to the expansion of strengthened WNPSH in the modified BMJ-applied runs. We showed that CPS working is reduced by changing the two factors in the BMJ scheme, resulting in the reduction of convective processes that occur excessively around typhoons at low latitudes. Additionally, we tried to change the values of the two factors a bit differently. We applied them to three typhoon cases with the large track spread (e.g., Noru, Trami, and Tapha) to identify the effect of changing the two parameters. As a result, we found that the best performances were shown when using the two values in Table 2 for the modified BMJ scheme, and better performance than the BMJ-applied runs was only simulated when excessive CPS activities at low latitudes were significantly reduced.

4. Summary and Conclusions

This study shows that typhoon track forecast performances largely depended on the applied physics combinations. On average, the best combination of physics options for typhoon forecasting in our model setting was found to be the KF scheme for CPS and WSM6 scheme for MPS. BMJ-applied runs showed the worst performances, and simulated typhoons tended to move significantly westward compared with other runs. In addition, P3-applied runs tended to overestimate the simulated typhoon intensities. We found that the reason why P3 scheme results in always stronger typhoons were due to the more enhanced formation of ice by the strong upward motion and increased latent heat release in the upper deep convection mainly by the vapor deposition process. Moreover, the simulated typhoon track (intensity) was largely affected by the applied CPS (MPS). Furthermore, excessive activation of CPS at low latitudes could significantly influence short-term typhoon forecasting performance by weakening the WNPSH. The BMJ scheme tended to be modulated very sensitively and allowed extensive precipitation, especially at low latitudes, resulting in less MPS-induced precipitation in the same region. The main issue with the BMJ scheme was the reference profiles, which were already determined based on mean structures observed in the deep convection. The BMJ scheme has been reported to have good performance (Athukorala et al., 2021; Choi & Ahn, 2017; Doutreloup et al., 2019; Evans et al., 2012; Kumar et al., 2014; Ratna et al., 2014) and widely used within the WRF community since it requires fewer computational resources due to its simplicity. However, our results show that the predetermined reference profiles could cause issues even in short-term typhoon forecasts. Thus, we suggest that the use of the BMJ scheme needs to be considered carefully in the WNP region or the scheme should be at least modified.

We found that some of the findings in this study were somewhat different from the previous studies due to the model setting or selected typhoon case. For example, in the study by Sun et al. (2014), they investigated the sensitivity of two CPSs on the simulation of typhoon Megi (2010) using the WRF model with a 20 km horizontal resolution domain. In their study, the WNPSH weakened and caused westward typhoon track errors when the BMJ scheme was applied. The initial WNPSH strengths were the same in their sensitivity experiments, but the WNPSH strength changed as the typhoon approached the WNPSH. These results seemed to be strongly related to the simulated spiral rainband in the BMJ-applied run was much stronger and distributed up to 30°N, where the WNPSH was separated. Thus, the contracted WNPSH due to the over-intensification of the simulated typhoon might be the reason for the strong westward bias in their study. However, in our study, the WNPSH was relatively contracted in BMJ-applied runs from the initial forecast time, and the simulated typhoon track was relatively less affected by the WNPSH than KF or TDK-applied runs. In addition, in the study by Biswas et al. (2014), they argued that simulated typhoon intensities were sensitive to the choice of the CPSs. However, when looking at the Faxai case in our study, there was an MWS difference of about 7 m s^{-1} among the CPSs, but in the study by Biswas et al. (2014), the largest 72-hr forecasted average intensity spread was only about 5 m s^{-1} . Although there was a difference in typhoon intensity among the CPSs in this study as in Biswas et al. (2014), this study does not emphasize much because the difference in typhoon intensity by MPSs was much more significant, and we kept emphasizing that those results may be closely related to the test of small number of CPSs and MPSs or our model setting.

There are a few further points worth noting, although some meaningful results were found in this study: to find the optimal choice of CPS and MPS for forecasting the recent landfalling typhoon cases, to show the impact of CPS and MPS on selected typhoon forecast, and to find the reason of large track forecast errors in BMJ-applied runs by modifying the reference profiles in the BMJ scheme. Firstly, the best physics combination proposed in this study is strongly influenced by our model settings (i.e., domain size, horizontal resolution, and physics scheme) and selected typhoon cases. In particular, our model was designed to predict typhoons affecting Korea,

so the results might be different when using our optimized physics setting for forecasting other typhoon cases in different model configurations. In addition, due to the parent domain that was designed to be focused largely on the WNPSH simulation, the mid-latitude trough was not sensitively simulated in all experiments. To address those issues, additional sensitivity studies for various typhoon cases and mid-latitude troughs by varying the parent domain are required. Secondly, our focus was to improve the forecast performances of selected typhoon cases in terms of the role of physics parameterization schemes. However, only a small number of cumulus parameterization and cloud microphysics schemes were tested in this study, so there is a need to conduct more sensitivity experiments using diverse kinds of physics parameterization schemes in the future for a more sophisticated forecast performance verification. Besides, various methods to achieve better performances in typhoon forecast have been introduced by lots of studies; increasing the model horizontal resolutions (Buizza, 2010; Davis et al., 2010), improving initial condition (Cha & Wang, 2013; Y. Choi, Cha, & Kim, 2017; Kurihara et al., 1993; Liu & Tan, 2016), using alternative boundary condition (Moon et al., 2018), and reflecting the realistic atmosphere and ocean interactions by using atmospheric-ocean coupled models (Bielli et al., 2021; Kim et al., 2014; Mogensen et al., 2017; Yesubabu et al., 2020). Therefore, other factors also should be considered and included in future studies with optimal physics combinations to further improve the overall typhoon forecast.

Data Availability Statement

Software—The Weather Research and Forecasting (WRF) model v4.1.2 is available at <https://www2.mmm.ucar.edu> (WRF, 2008). Figures have been made with the National Center for Atmospheric Research (NCAR) Command Language (NCL v6.5.0) post-processing tool accessible at <https://www.ncl.ucar.edu> (NCL, 2019). Data—The meteorological input data to create the initial and boundary conditions for the WRF model domains were obtained from the Global Forecast System (GFS) forecast and analysis data available at the National Centers for Environmental Information (NCEI) online at <http://ncei.noaa.gov> (GFS, 2015). The WRF simulation data can be accessed on the Zenodo repository (<https://doi.org/10.5281/zenodo.7024346>) (Park et al., 2022).

Acknowledgments

This research was supported by the Carbon Neutral Institute Research Fund (Project No. 1.220093.01) of UNIST (Ulsan National Institute of Science & Technology), and in part carried out through the R&D project “Development of the Next-generation Operational System of Korea Institute of Atmospheric Prediction Systems (KIAPS)”, funded by Korea Meteorological Administration (KMA2020-02213).

References

- Arakawa, A. (2004). The cumulus parameterization problem: Past, present, and future. *Journal of Climate*, 17(13), 2493–2525. [https://doi.org/10.1175/1520-0442\(2004\)017<2493:ratcpp>2.0.co;2](https://doi.org/10.1175/1520-0442(2004)017<2493:ratcpp>2.0.co;2)
- Athukorala, R., Thol, T., Neluwala, P., Petri, M., Sengxue, S., Lattada, L., et al. (2021). Evaluating the performance of a WRF physics ensemble in simulating rainfall over Lao PDR during wet and dry seasons. *Advances in Meteorology*, 2021, 1–16. <https://doi.org/10.1155/2021/6630302>
- Betts, A. K., & Miller, M. J. (1986). A new convective adjustment scheme. Part II: Single column tests using GATE wave, BOMEX, ATEX and arctic air-mass data sets. *Quarterly Journal of the Royal Meteorological Society*, 112(473), 693–709. <https://doi.org/10.1256/smsqj.47307>
- Bielli, S., Barthe, C., Bousquet, O., Tulet, P., & Pianezze, J. (2021). The effect of atmosphere–ocean coupling on the structure and intensity of tropical cyclone Bejisa in the southwest Indian Ocean. *Atmosphere*, 12(6), 688. <https://doi.org/10.3390/atmos12060688>
- Biswas, M. K., Bernardet, L., & Dudhia, J. (2014). Sensitivity of hurricane forecasts to cumulus parameterizations in the HWRF model. *Geophysical Research Letters*, 41(24), 9113–9119. <https://doi.org/10.1002/2014gl062071>
- Braun, S. A., & Tao, W.-K. (2000). Sensitivity of high-resolution simulations of Hurricane Bob (1991) to planetary boundary layer parameterizations. *Monthly Weather Review*, 128(12), 3941–3961. [https://doi.org/10.1175/1520-0493\(2000\)129<3941:sohrso>2.0.co;2](https://doi.org/10.1175/1520-0493(2000)129<3941:sohrso>2.0.co;2)
- Buizza, R. (2010). Horizontal resolution impact on short- and long-range forecast error. *Quarterly Journal of the Royal Meteorological Society*, 136(649), 1020–1035. <https://doi.org/10.1002/qj.613>
- Cangialosi, J. P. (2020). National Hurricane Center forecast verification report.
- Carr, L. E., III. (1989). Barotropic vortex adjustment to asymmetric forcing with application to tropical cyclone motion.
- Carr, L. E., III, & Elsberry, R. L. (1997). Models of tropical cyclone wind distribution and beta-effect propagation for application to tropical cyclone track forecasting. *Monthly Weather Review*, 125(12), 3190–3209. [https://doi.org/10.1175/1520-0493\(1997\)125<3190:motcwid>2.0.co;2](https://doi.org/10.1175/1520-0493(1997)125<3190:motcwid>2.0.co;2)
- Cha, D.-H., & Wang, Y. (2013). A dynamical initialization scheme for real-time forecasts of tropical cyclones using the WRF model. *Monthly Weather Review*, 141(3), 964–986. <https://doi.org/10.1175/mwr-d-12-00077.1>
- Cha, Y., Choi, K.-S., Chang, K.-H., Lee, J.-Y., & Shin, D.-S. (2014). Characteristics of the changes in tropical cyclones influencing the South Korean region over the recent 10 years (2001–2010). *Natural Hazards*, 74(3), 1729–1741. <https://doi.org/10.1007/s11069-014-1275-4>
- Chang, M., Park, D.-S. R., & Ho, C.-H. (2021). Possible cause of seasonal inhomogeneity in interdecadal changes of tropical cyclone Genesis frequency over the Western North Pacific. *Journal of Climate*, 34(2), 635–642. <https://doi.org/10.1175/jcli-d-20-0268.1>
- Chen, G., Yu, H., & Cao, Q. (2015). Evaluation of tropical cyclone forecasts from operational global models over the Western North Pacific in 2013. *Tropical Cyclone Research and Review*, 4(1), 18–26.
- Chen, G., Zhang, X., Bai, L., & Wan, R. (2019). Verification of tropical cyclone operational forecast in 2018. *Proceedings of the ESCAP/WMO Typhoon Committee, Guangzhou, China*, 26.
- Choi, J.-W., Cha, Y., & Kim, J.-Y. (2017). Interdecadal variation of Korea affecting TC activity in early 1980s. *Geoscience Letters*, 4(1), 1–7. <https://doi.org/10.1186/s40562-017-0068-5>
- Choi, K.-S., & Kim, B.-J. (2007). Climatological characteristics of tropical cyclones making landfall over the Korean Peninsula. *Asia-Pacific Journal of Atmospheric Sciences*, 43(2), 13–25.
- Choi, K.-S., & Moon, I.-J. (2012). Changes in tropical cyclone activity that has affected Korea since 1999. *Natural Hazards*, 62(3), 971–989. <https://doi.org/10.1007/s11069-012-0131-7>

- Choi, Y., Cha, D. H., Lee, M. I., Kim, J., Jin, C. S., Park, S. H., & Joh, M. S. (2017). Satellite radiance data assimilation for binary tropical cyclone cases over the Western North Pacific. *Journal of Advances in Modeling Earth Systems*, 9(2), 832–853. <https://doi.org/10.1002/2016ms000826>
- Choi, Y.-W., & Ahn, J.-B. (2017). Impact of cumulus parameterization schemes on the regional climate simulation for the domain of CORDEX--East Asia phase 2 using WRF model. *Atmosphere*, 27(1), 105–118. <https://doi.org/10.14191/atmos.2017.27.1.105>
- Davis, C., Wang, W., Dudhia, J., & Torn, R. (2010). Does increased horizontal resolution improve hurricane wind forecasts? *Weather and Forecasting*, 25(6), 1826–1841. <https://doi.org/10.1175/2010waf2222423.1>
- DeMaria, M., Franklin, J. L., Onderlinde, M. J., & Kaplan, J. (2021). Operational forecasting of tropical cyclone rapid intensification at the National Hurricane Center. *Atmosphere*, 12(6), 683. <https://doi.org/10.3390/atmos12060683>
- Doutreloup, S., Wyard, C., Amory, C., Kittel, C., Erpicum, M., & Fettweis, X. (2019). Sensitivity to convective schemes on precipitation simulated by the regional climate model MAR over Belgium (1987–2017). *Atmosphere*, 10(1), 34. <https://doi.org/10.3390/atmos10010034>
- Dudhia, J. (1989). Numerical study of convection observed during the winter monsoon experiment using a mesoscale two-dimensional model. *Journal of the Atmospheric Sciences*, 46(20), 3077–3107. [https://doi.org/10.1175/1520-0469\(1989\)046<3077:nsocod>2.0.co;2](https://doi.org/10.1175/1520-0469(1989)046<3077:nsocod>2.0.co;2)
- Dudhia, J. (1993). A nonhydrostatic version of the Penn State–NCAR mesoscale model: Validation tests and simulation of an Atlantic cyclone and cold front. *Monthly Weather Review*, 121(5), 1493–1513. [https://doi.org/10.1175/1520-0493\(1993\)121<1493:anvotp>2.0.co;2](https://doi.org/10.1175/1520-0493(1993)121<1493:anvotp>2.0.co;2)
- Elsberry, R. L., Lambert, T. D., & Boothe, M. A. (2007). Accuracy of Atlantic and eastern North Pacific tropical cyclone intensity forecast guidance. *Weather and Forecasting*, 22(4), 747–762. <https://doi.org/10.1175/waf1015.1>
- Elsner, J. B., Kossin, J. P., & Jagger, T. H. (2008). The increasing intensity of the strongest tropical cyclones. *Nature*, 455(7209), 92–95. <https://doi.org/10.1038/nature07234>
- Evans, J. P., Ekström, M., & Ji, F. (2012). Evaluating the performance of a WRF physics ensemble over South-East Australia. *Climate Dynamics*, 39(6), 1241–1258. <https://doi.org/10.1007/s00382-011-1244-5>
- Fang, J., & Zhang, F. (2012). Effect of beta shear on simulated tropical cyclones. *Monthly Weather Review*, 140(10), 3327–3346. <https://doi.org/10.1175/mwr-d-10-05021.1>
- Fiorino, M., & Elsberry, R. L. (1989). Some aspects of vortex structure related to tropical cyclone motion. *Journal of the Atmospheric Sciences*, 46(7), 975–990. [https://doi.org/10.1175/1520-0469\(1989\)046<0975:saovrs>2.0.co;2](https://doi.org/10.1175/1520-0469(1989)046<0975:saovrs>2.0.co;2)
- Fonseca, R., Zhang, T., & Yong, K.-T. (2015). Improved simulation of precipitation in the tropics using a modified BMJ scheme in the WRF model. *Geoscientific Model Development*, 8(9), 2915–2928. <https://doi.org/10.5194/gmd-8-2915-2015>
- Fovell, R. G., & Su, H. (2007). Impact of cloud microphysics on hurricane track forecasts. *Geophysical Research Letters*, 34(24), L24810. <https://doi.org/10.1029/2007gl031723>
- GFS. (2015). NCEP GDAS/FNL 0.25 degree global tropospheric analyses and forecast grids [Dataset]. Retrieved from <https://rda.ucar.edu/datasets/ds083.3/index.html#!description>
- Goerss, J. S. (2007). Prediction of consensus tropical cyclone track forecast error. *Monthly Weather Review*, 135(5), 1985–1993. <https://doi.org/10.1175/mwr3390.1>
- Gopalakishnan, S., Upadhayay, S., Jung, Y., Marks, F., Tallapragada, V., Mehra, A., et al. (2021). 2020 HFIP R&D activities summary: Recent results and operational implementation.
- Grell, G. A., Dudhia, J., & Stauffer, D. R. (1994). A description of the fifth-generation Penn state/NCAR Mesoscale model (MM5).
- Heming, J. T., Prates, F., Bender, M. A., Bowyer, R., Cangialosi, J., Caroff, P., et al. (2019). Review of recent progress in tropical cyclone track forecasting and expression of uncertainties. *Tropical Cyclone Research and Review*, 8(4), 181–218. <https://doi.org/10.1016/j.tcr.2020.01.001>
- Holland, G., & Bruyère, C. L. (2014). Recent intense hurricane response to global climate change. *Climate Dynamics*, 42(3), 617–627. <https://doi.org/10.1007/s00382-013-1713-0>
- Hong, S.-Y., & Lim, J.-O. J. (2006). The WRF single-moment 6-class microphysics scheme (WSM6). *Asia-Pacific Journal of Atmospheric Sciences*, 42(2), 129–151.
- Hong, S.-Y., Noh, Y., & Dudhia, J. (2006). A new vertical diffusion package with an explicit treatment of entrainment processes. *Monthly Weather Review*, 134(9), 2318–2341. <https://doi.org/10.1175/mwr3199.1>
- Huang, X., Peng, X., Fei, J., Cheng, X., Ding, J., & Yu, D. (2021). Evaluation and error analysis of official tropical cyclone intensity forecasts during 2005–2018 for the Western North Pacific. *Journal of the Meteorological Society of Japan*, 119(1), 139–163. <https://doi.org/10.2151/jmsj.2021-008>
- Janjić, Z. I. (1994). The step-mountain eta coordinate model: Further developments of the convection, viscous sublayer, and turbulence closure schemes. *Monthly Weather Review*, 122(5), 927–945. [https://doi.org/10.1175/1520-0493\(1994\)122<0927:tsmecom>2.0.co;2](https://doi.org/10.1175/1520-0493(1994)122<0927:tsmecom>2.0.co;2)
- Kain, J. S. (2004). The Kain–Fritsch convective parameterization: An update. *Journal of Applied Meteorology*, 43(1), 170–181. [https://doi.org/10.1175/1520-0450\(2004\)043<0170:tkepau>2.0.co;2](https://doi.org/10.1175/1520-0450(2004)043<0170:tkepau>2.0.co;2)
- Kim, B.-J. (2008). A climatological feature of typhoon making landfall over the Korean Peninsula. *Paper Presented at the 20th Conference on Climate Variability and Change*.
- Kim, H.-S., Lozano, C., Tallapragada, V., Iredell, D., Sheinin, D., Tolman, H. L., et al. (2014). Performance of ocean simulations in the coupled HWRF–HYCOM model. *Journal of Atmospheric and Oceanic Technology*, 31(2), 545–559. <https://doi.org/10.1175/jtech-d-13-00013.1>
- Knutson, T. R., McBride, J. L., Chan, J., Emanuel, K., Holland, G., Landsea, C., et al. (2010). Tropical cyclones and climate change. *Nature Geoscience*, 3(3), 157–163. <https://doi.org/10.1038/ngeo779>
- Kumar, S., Routray, A., Chauhan, R., & Panda, J. (2014). Impact of parameterization schemes and 3DVAR data assimilation for simulation of heavy rainfall events along west coast of India with WRF modeling system. *International Journal of Earth and Atmospheric Science*, 1(1), 18–34.
- Kurihara, Y., Bender, M. A., & Ross, R. J. (1993). An initialization scheme of hurricane models by vortex specification. *Monthly Weather Review*, 121(7), 2030–2045. [https://doi.org/10.1175/1520-0493\(1993\)121<2030:aisohm>2.0.co;2](https://doi.org/10.1175/1520-0493(1993)121<2030:aisohm>2.0.co;2)
- Landsea, C. W., & Cangialosi, J. P. (2018). Have we reached the limits of predictability for tropical cyclone track forecasting? *Bulletin of the American Meteorological Society*, 99(11), 2237–2243. <https://doi.org/10.1175/bams-d-17-0136.1>
- Lee, M., Cha, D. H., Moon, J., Park, J., Jin, C. S., & Chan, J. C. (2019). Long-term trends in tropical cyclone tracks around Korea and Japan in late summer and early fall. *Atmospheric Science Letters*, 20(11), e939. <https://doi.org/10.1002/asl.939>
- Lee, T.-C., Knutson, T. R., Kamahori, H., & Ying, M. (2012). Impacts of climate change on tropical cyclones in the Western North Pacific basin. Part I: Past observations. *Tropical Cyclone Research and Review*, 1(2), 213–235.
- Li, Q., Chen, C., Yu, J., & Chen, L. (2012). Evaluating the performance of Western North Pacific tropical cyclone intensity guidance. Part II: Intensity forecast accuracy in different life stages. *Tropical Cyclone Research and Review*, 1(4), 458–468.
- Liu, H.-Y., & Tan, Z.-M. (2016). A dynamical initialization scheme for binary tropical cyclones. *Monthly Weather Review*, 144(12), 4787–4803. <https://doi.org/10.1175/mwr-d-16-0176.1>

- Liu, L., Wang, Y., Zhan, R., Xu, J., & Duan, Y. (2020). Increasing destructive potential of landfalling tropical cyclones over China. *Journal of Climate*, 33(9), 3731–3743. <https://doi.org/10.1175/jcli-d-19-0451.1>
- Lord, S. J., Willoughby, H. E., & Piotrowicz, J. M. (1984). Role of a parameterized ice-phase microphysics in an axisymmetric, nonhydrostatic tropical cyclone model. *Journal of the Atmospheric Sciences*, 41(19), 2836–2848. [https://doi.org/10.1175/1520-0469\(1984\)041<2836:roaip>2.0.co;2](https://doi.org/10.1175/1520-0469(1984)041<2836:roaip>2.0.co;2)
- Mlawer, E. J., Taubman, S. J., Brown, P. D., Iacono, M. J., & Clough, S. A. (1997). Radiative transfer for inhomogeneous atmospheres: RRTM, a validated correlated-k model for the longwave. *Journal of Geophysical Research*, 102(D14), 16663–16682. <https://doi.org/10.1029/97jd00237>
- Mogensen, K. S., Magnusson, L., & Bidlot, J. R. (2017). Tropical cyclone sensitivity to ocean coupling in the ECMWF coupled model. *Journal of Geophysical Research: Oceans*, 122(5), 4392–4412. <https://doi.org/10.1002/2017jc012753>
- Moon, J., Cha, D. H., Lee, M., & Kim, J. (2018). Impact of spectral nudging on real-time tropical cyclone forecast. *Journal of Geophysical Research: Atmospheres*, 123(22), 12647–12660. <https://doi.org/10.1029/2018jd028550>
- Moon, J., Park, J., & Cha, D.-H. (2021). Does increasing model resolution improve the real-time forecasts of Western North Pacific tropical cyclones? *Atmosphere*, 12(6), 776. <https://doi.org/10.3390/atmos12060776>
- Moon, J., Park, J., Cha, D.-H., & Moon, Y. (2021). Five-day track forecast skills of WRF model for the Western North Pacific tropical cyclones. *Weather and Forecasting*, 36(4), 1491–1503. <https://doi.org/10.1175/waf-d-20-0092.1>
- Morrison, H., Milbrandt, J. A., Bryan, G. H., Ikeda, K., Tessendorf, S. A., & Thompson, G. (2015). Parameterization of cloud microphysics based on the prediction of bulk ice particle properties. Part II: Case study comparisons with observations and other schemes. *Journal of the Atmospheric Sciences*, 72(1), 312–339. <https://doi.org/10.1175/jas-d-14-0066.1>
- Munsell, E. B., Sippel, J. A., Braun, S. A., Weng, Y., & Zhang, F. (2015). Dynamics and predictability of Hurricane Nadine (2012) evaluated through convection-permitting ensemble analysis and forecasts. *Monthly Weather Review*, 143(11), 4514–4532. <https://doi.org/10.1175/mwr-d-14-00358.1>
- Murakami, H., Vecchi, G. A., Underwood, S., Delworth, T. L., Wittenberg, A. T., Anderson, W. G., et al. (2015). Simulation and prediction of category 4 and 5 hurricanes in the high-resolution GFDL HiFLOR coupled climate model. *Journal of Climate*, 28(23), 9058–9079. <https://doi.org/10.1175/jcli-d-15-0216.1>
- Murakami, H., Wang, Y., Yoshimura, H., Mizuta, R., Sugi, M., Shindo, E., et al. (2012). Future changes in tropical cyclone activity projected by the new high-resolution MRI-AGCM. *Journal of Climate*, 25(9), 3237–3260. <https://doi.org/10.1175/jcli-d-11-00415.1>
- Na, W., McBride, J. L., Zhang, X.-H., & Duan, Y.-H. (2018). Understanding biases in tropical cyclone intensity forecast error. *Weather and Forecasting*, 33(1), 129–138. <https://doi.org/10.1175/waf-d-17-0106.1>
- NCL. (2019). The NCAR command language. Software. <https://doi.org/10.5065/D6WD3XHS>
- Noh, Y., Cheon, W., Hong, S., & Raasch, S. (2003). Improvement of the K-profile model for the planetary boundary layer based on large eddy simulation data. *Boundary-Layer Meteorology*, 107(2), 401–427. <https://doi.org/10.1023/a:1022146015946>
- Park, D.-S. R., Ho, C.-H., & Kim, J.-H. (2014). Growing threat of intense tropical cyclones to East Asia over the period 1977–2010. *Environmental Research Letters*, 9(1), 014008. <https://doi.org/10.1088/1748-9326/9/1/014008>
- Park, J., Cha, D. H., Lee, M. K., Moon, J., Hahm, S. J., Noh, K., et al. (2020). Impact of cloud microphysics schemes on tropical cyclone forecast over the Western North Pacific. *Journal of Geophysical Research: Atmospheres*, 125(18), e2019JD032288. <https://doi.org/10.1029/2019jd032288>
- Park, J., Moon, J., Cho, W., Cha, D.-H., Lee, M.-I., Chang, E.-C., et al. (2022). WRF simulation data [Dataset]. Zenodo. <https://doi.org/10.5281/zenodo.7024346>
- Ratna, S. B., Ratnam, J., Behera, S., Rautenbach, C. d., Ndarana, T., Takahashi, K., & Yamagata, T. (2014). Performance assessment of three convective parameterization schemes in WRF for downscaling summer rainfall over South Africa. *Climate Dynamics*, 42(11), 2931–2953. <https://doi.org/10.1007/s00382-013-1918-2>
- Sakai, R., & Yamaguchi, M. (2005). The WGENE intercomparison of tropical cyclone track forecasts by operational global models. *CAS/JSC WGENE Research Activities in Atmospheric and Oceanic Modeling*, 35, 0207–0208.
- Shepherd, T. J., & Walsh, K. J. (2017). Sensitivity of hurricane track to cumulus parameterization schemes in the WRF model for three intense tropical cyclones: Impact of convective asymmetry. *Meteorology and Atmospheric Physics*, 129(4), 345–374. <https://doi.org/10.1007/s00703-016-0472-y>
- Skamarock, W. C., Klemp, J. B., Dudhia, J., Gill, D. O., Liu, Z., Berner, J., et al. (2019). *A description of the advanced research WRF model version 4*. National Center for Atmospheric Research.145
- Smith, R. K., & Thomsen, G. L. (2010). Dependence of tropical-cyclone intensification on the boundary-layer representation in a numerical model. *Quarterly Journal of the Royal Meteorological Society*, 136(652), 1671–1685. <https://doi.org/10.1002/qj.687>
- Sun, Y., Zhong, Z., Lu, W., & Hu, Y. (2014). Why are tropical cyclone tracks over the Western North Pacific sensitive to the cumulus parameterization scheme in regional climate modeling? A case study for Megi (2010). *Monthly Weather Review*, 142(3), 1240–1249. <https://doi.org/10.1175/mwr-d-13-00232.1>
- Tang, C. K., Chan, J. C., & Yamaguchi, M. (2021). Large tropical cyclone track forecast errors of global numerical weather prediction models in Western North Pacific Basin. *Tropical Cyclone Research and Review*. <https://doi.org/10.1016/j.tcr.2021.07.001>
- Tiedtke, M. (1989). A comprehensive mass flux scheme for cumulus parameterization in large-scale models. *Monthly Weather Review*, 117(8), 1779–1800. [https://doi.org/10.1175/1520-0493\(1989\)117<1779:acmfsf>2.0.co;2](https://doi.org/10.1175/1520-0493(1989)117<1779:acmfsf>2.0.co;2)
- Trabing, B. C., & Bell, M. M. (2020). Understanding error distributions of hurricane intensity forecasts during rapid intensity changes. *Weather and Forecasting*, 35(6), 2219–2234. <https://doi.org/10.1175/waf-d-19-0253.1>
- Tu, J.-Y., Chou, C., & Chu, P.-S. (2009). The abrupt shift of typhoon activity in the vicinity of Taiwan and its association with Western North Pacific–East Asian climate change. *Journal of Climate*, 22(13), 3617–3628. <https://doi.org/10.1175/2009jcli2411.1>
- Wang, Y. (2002). An explicit simulation of tropical cyclones with a triply nested movable mesh primitive equation model: TCM3. Part II: Model refinements and sensitivity to cloud microphysics parameterization. *Monthly Weather Review*, 130(12), 3022–3036. [https://doi.org/10.1175/1520-0493\(2002\)130<3022:aesotc>2.0.co;2](https://doi.org/10.1175/1520-0493(2002)130<3022:aesotc>2.0.co;2)
- Webster, P. J., Holland, G. J., Curry, J. A., & Chang, H.-R. (2005). Changes in tropical cyclone number, duration, and intensity in a warming environment. *Science*, 309(5742), 1844–1846. <https://doi.org/10.1126/science.1116448>
- Wood, K. M., & Ritchie, E. A. (2015). A definition for rapid weakening of North Atlantic and eastern North Pacific tropical cyclones. *Geophysical Research Letters*, 42(22), 10091–10097. <https://doi.org/10.1002/2015gl066697>
- WRF. (2008). A description of the advanced research WRF version 3. Software. Retrieved from https://www2.mmm.ucar.edu/wrf/users/download/get_source.html
- Wu, L., Wang, B., & Geng, S. (2005). Growing typhoon influence on East Asia. *Geophysical Research Letters*, 32(18). <https://doi.org/10.1029/2005gl022937>

- Wu, L., & Zhao, H. (2012). Dynamically derived tropical cyclone intensity changes over the Western North Pacific. *Journal of Climate*, 25(1), 89–98. <https://doi.org/10.1175/2011jcli4139.1>
- Xu, W., Qi, L., Du, Y., & Xia, L. (2016). Analysis on abnormal tropical cyclone track forecast error of ECMWF-IFS in the Western North Pacific. *Tropical Cyclone Research and Review*, 5(1–2), 12–22.
- Yamada, H., Nasuno, T., Yanase, W., & Satoh, M. (2016). Role of the vertical structure of a simulated tropical cyclone in its motion: A case study of typhoon Fengshen (2008). *SOLA*, 12(0), 203–208. <https://doi.org/10.2151/sola.2016-041>
- Yamaguchi, M., Ishida, J., Sato, H., & Nakagawa, M. (2017). WGNE intercomparison of tropical cyclone forecasts by operational NWP models: A quarter century and beyond. *Bulletin of the American Meteorological Society*, 98(11), 2337–2349. <https://doi.org/10.1175/bams-d-16-0133.1>
- Yesubabu, V., Kattamanchi, V. K., Vissa, N. K., Dasari, H. P., & Sarangam, V. B. R. (2020). Impact of ocean mixed-layer depth initialization on the simulation of tropical cyclones over the Bay of Bengal using the WRF-ARW model. *Meteorological Applications*, 27(1), e1862. <https://doi.org/10.1002/met.1862>
- Zhang, C., Wang, Y., & Hamilton, K. (2011). Improved representation of boundary layer clouds over the southeast Pacific in ARW-WRF using a modified Tiedtke cumulus parameterization scheme. *Monthly Weather Review*, 139(11), 3489–3513. <https://doi.org/10.1175/mwr-d-10-05091.1>
- Zhou, X., Zhu, Y., Hou, D., Luo, Y., Peng, J., & Wobus, R. (2017). Performance of the new NCEP global ensemble forecast system in a parallel experiment. *Weather and Forecasting*, 32(5), 1989–2004. <https://doi.org/10.1175/waf-d-17-0023.1>
- Zhu, T., & Zhang, D.-L. (2006). Numerical simulation of Hurricane Bonnie (1998). Part II: Sensitivity to varying cloud microphysical processes. *Journal of the Atmospheric Sciences*, 63(1), 109–126. <https://doi.org/10.1175/jas3599.1>